



## 저작자표시-비영리-변경금지 2.0 대한민국

이용자는 아래의 조건을 따르는 경우에 한하여 자유롭게

- 이 저작물을 복제, 배포, 전송, 전시, 공연 및 방송할 수 있습니다.

다음과 같은 조건을 따라야 합니다:



저작자표시. 귀하는 원저작자를 표시하여야 합니다.



비영리. 귀하는 이 저작물을 영리 목적으로 이용할 수 없습니다.



변경금지. 귀하는 이 저작물을 개작, 변형 또는 가공할 수 없습니다.

- 귀하는, 이 저작물의 재이용이나 배포의 경우, 이 저작물에 적용된 이용허락조건을 명확하게 나타내어야 합니다.
- 저작권자로부터 별도의 허가를 받으면 이러한 조건들은 적용되지 않습니다.

저작권법에 따른 이용자의 권리는 위의 내용에 의하여 영향을 받지 않습니다.

이것은 [이용허락규약\(Legal Code\)](#)을 이해하기 쉽게 요약한 것입니다.

[Disclaimer](#)

의학박사 학위논문

Efficacy of Hydroxyapatite Gradient  
Extracellular Matrix Scaffold Seeded with  
Umbilical Cord-Derived Mesenchymal  
Stem Cells on Regeneration of  
Tendon-to-Bone Interface of Rotator Cuff

제대유래 중간엽 줄기세포를 적용한  
수산화인회석 농도 경사 세포외기질  
스캐폴드의 회전근개 건-골 접합부 재생 효과

2021년 2월

서울대학교 대학원  
의학과 중개의학 전공  
예 지 혜

제대유래 중간엽 줄기세포를 적용한  
수산화인회석 농도 경사 세포외기질  
스캐폴드의 회전근개 건-골 접합부 재생 효과

지도교수 조 현 철

이 논문을 의학박사 학위논문으로 제출함

2020년 10월


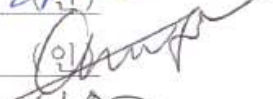
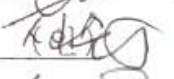
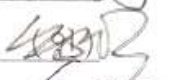
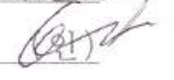
서울대학교 대학원

의학과 중개의학전공

예 지 혜

예지혜의 박사 학위논문을 인준함

2021년 1월

위 원 장	김 상 완	
부 위 원 장	김 준 하	
위 원	신 수	
위 원	홍 문 호	
위 원	배 태 우	

Efficacy of Hydroxyapatite Gradient  
Extracellular Matrix Scaffold Seeded with  
Umbilical Cord-Derived Mesenchymal Stem  
Cells on Regeneration of Tendon-to-Bone  
Interface of Rotator Cuff

by Ji-Hye Yea

(Directed by Chris Hyunchul Jo, MD, PhD)

A thesis submitted in partial fulfillment of the  
requirements for the degree of Doctor of Philosophy in  
Translational Medicine at Seoul National University  
College of Medicine

January 2021

Approved by thesis committee:

Professor	<u>Sang Wan Kim</u>	Chairman
Professor	<u>Chris Jo</u>	Vice chairman
Professor	<u>Sue SHIN.</u>	
Professor	<u>YOUNG HO HONG.</u>	
Professor	<u>Bae Tae Goo</u>	

## Abstract

# Efficacy of Hydroxyapatite Gradient Extracellular Matrix Scaffold Seeded with Umbilical Cord-Derived Mesenchymal Stem Cells on Regeneration of Tendon-to-Bone Interface of Rotator Cuff

Ji-Hye Yea

Department of Medicine, Translational Medicine

The Graduate School

Seoul National University

Regeneration of the gradient structure of the tendon-to-bone interface (TBI) is a crucial goal after rotator cuff repair. The purpose of this study was to investigate the efficacy of a biomimetic hydroxyapatite-gradient (HA-G) scaffold made from adipose tissue (AD) with umbilical cord-derived mesenchymal stem cells (UC MSCs) on the regeneration of the gradient structure of the TBI by analyzing the histological and biomechanical changes in a rat repair model.

To mimic the structure of TBI, I prepared a scaffold consisting of

extracellular matrix made from human AD and covered by chondroitin sulfate. Then, the scaffold was formed progressively increased hydroxyapatite (HA) particles from the tendon to the bone phase. The fabricated HA-G scaffold had high interconnectivity of structure, 100-150 $\mu$ m pore size, and 91% porosity. Compared to tendon phase, the proportion of inorganic material such as HA was higher by 1.4-fold and 2.9-fold and the mechanical strength was also enhanced by 1.5-fold and 2.3-fold in cartilage and bone phase respectively.

When UC MSCs were implanted to the HA-G scaffold, the UC MSCs adhered to the surface of tendon and bone phases, and the adhesion rate was 98% at 24 hours. At 7 days, the cells migrated to the middle side (cartilage phase) and the cells were evenly distributed on the tendon, cartilage and bone sides at 14 days. The cells proliferated 6-fold at 21 days compared to that at 1 day. In histological evaluation, UC MSC seeded HA-G scaffold had significantly higher the collagen deposit by 2.9-fold on tendon phase, glycosaminoglycan (GAG) deposit by 6.3-fold on cartilage phase and calcium deposit by 5.4-fold on bone phase respectively than those in HA-G scaffold without UC MSCs (all  $p < 0.001$ ).

Compared to the repair group in a rotator cuff repair rat model, the UC MSCs seeded HA-G scaffold group had significantly increased maturing score by 1.2-fold at 8 weeks ( $p = 0.021$ ). Collagen organization and cartilage formation were also improved by 1.6-fold at 8 weeks and by 3.8-fold at 4 weeks, respectively. Especially, the

tidemark, which could be observed after cartilage maturation, was recovered 14% in UC MSCs seeded HA-G scaffold group at 8 weeks whereas it was not found in the repair group. Moreover, ultimate failure load also significantly increased by 1.3-fold at 4 weeks and 1.2-fold at 8 weeks in the UC MSCs seeded HA-G scaffold group compared to the repair group ( $p = 0.004$  and  $p = 0.049$  respectively). Compared to the repair group, the stiffness was also significantly improved by 1.7-fold in the UC MSCs seeded HA-G scaffold group at 8 weeks ( $p = 0.001$ ). Especially, the improved values were comparable to values in normal group.

This study demonstrated that HA-G scaffold made from AD seeded with UC MSCs formed tendon, cartilage and bone matrices similar to the TBI structure according to the HA density. Furthermore, UC MSC-seeded HA-G scaffold regenerated the TBI of the rotator cuff in a rat repair model in terms of histological and biomechanical properties similar to the normal TBI.

.....

**Keywords :** Shoulder pain, Rotator cuff, Tendon-to-bone interface, Umbilical cord, Mesenchymal stem cell, Gradient scaffold, Adipose tissue.

**Student number :** 2017-32957

## List of figures

<b>Figure 1</b>	Procedure of UC MSCs seeding to the HA-G scaffold.....	52
<b>Figure 2</b>	Surgical procedure of rotator cuff tendon repair.....	53
<b>Figure 3</b>	Characterization of the HA-G scaffold.....	54
<b>Figure 4</b>	Characterization of UC MSCs.....	55
<b>Figure 5</b>	Adhesion of UC MSCs to the HA-G scaffold.....	57
<b>Figure 6</b>	Infiltration, and proliferation of UC MSCs in the HA-G scaffold.....	58
<b>Figure 7</b>	Differentiation of UC MSCs in the HA-G scaffold at tendon, cartilage and bone phase at 28 days.....	60
<b>Figure 8</b>	Histologic image of the general structure, and quantification of the changes in the TBI at 4 and 8 weeks.....	61
<b>Figure 9</b>	Detail parameters of total regeneration score of TBI.....	62
<b>Figure 10</b>	Representative histologic images of the collagen matrix and quantification of the changes in the TBI at 4 and 8	



	weeks.....	63
<b>Figure 11</b>	Representative histologic images of cartilage and quantification of the changes in TBI at 4 and 8 weeks.....	64
<b>Figure 12</b>	Representative histologic images of tidemark and quantification of the changes in TBI at 4 and 8 weeks.....	65
<b>Figure 13</b>	Biomechanical test procedure and quantification of biomechanical properties of TBI at 4 and 8 weeks.....	66
<b>Figure 14</b>	Representative trafficking image of the human UC MSCs implanted within the TBI and quantification of the cells at 4 and 8 weeks.....	68

## List of abbreviations

AD	Adipose tissue
AD MSCs	Adipose tissue-derived mesenchymal stem cells
B	Bone phase
BM MSCs	Bone marrow-derived mesenchymal stem cells
C	Cartilage phase
CS	Chondroitin sulfate
DAPI	4'-6-diamidino-2-phenylindole
DPBS	Demineralized phosphate-buffered saline
ECM	Extracellular matrix
EDC	1-ethyl-3(3-dimethyl aminopropyl) carbodiimide
EDTA	Ethylenediaminetetraacetic acid
FBS	Fetal bovine serum
Fc	Calcified fibrocartilage
FTIR	Fourier-transform infrared
GAG	Glycosaminoglycan
HA	Hydroxyapatite
HA-G	Hydroxyapatite gradient
HE	Hematoxylin and eosin
IHC	Immunohistochemistry
MSCs,	Mesenchymal stem cells
MT	Masson's trichrome

PFA	Paraformaldehyde
PSR	Picrosirius red
Saf-O	Safranin-O/fast green
SDS	Sodium dodecyl sulfate
SEM	Scanning electron microscopy
SSM	Supraspinatus muscle
SST	Supraspinatus tendon
T	Tendon phase
TBI	Tendon-to-bone interface.
TGA	Thermogravimetric analysis
TM	Tendon muscular
UC MSCs	Umbilical cord-derived mesenchymal stem cells
U-Fc	Uncalcified fibrocartilage
WST	Water-soluble tetrazolium salt

# Contents

Abstract.....	i
List of figures.....	iv
List of abbreviations.....	vi
Contents.....	viii
I. Introduction.....	1
II. Materials and methods.....	6
1. Scaffold fabrication	
2. The HA-G scaffold characterization	
3. UC MSCs isolation and culture	
4. Characterization of UC MSCs	
5. UC MSCs seeding to the HA-G scaffold	
6. Adhesion and proliferation of UC MSCs in the HA-G scaffold	
7. Matrix formation of tendon, cartilage, and bone by UC MSCs	
8. In vivo study design	
9. Surgical procedures	
10. Histological evaluation	
11. Biomechanical evaluation	
12. UC MSCs trafficking	
13. Statistical analysis	
III. Results.....	24
1. Characterization of HA-G scaffolds	
2. Characterization of UC MSCs	
3. Adhesion, infiltration, and proliferation of UC MSCs in the	

HA-G scaffold	
4. Histological evaluation of differentiated UC MSCs in HA-G scaffold	
5. Histological evaluation of regenerated tendon	
6. Biomechanical properties of regenerated tendon	
7. Human cell tracking	
IV. Discussion.....	32
V. Conclusion.....	38
VI. References.....	39
국문초록.....	69

# I. Introduction

Shoulder pain is common musculoskeletal symptom and the prevalence of shoulder disorders is 7 to 34% of all general population (1). The most common cause of shoulder pain is rotator cuff tear, inducing substantial pain and impairing active motion (2). Surgery is used to treat rotator cuff tears, and more than 300,000 rotator cuff repair procedures are performed annually in the United States (3-5). Tendon to bone interface (TBI) of rotator cuff consists of four transitional zones such as the tendon, uncalcified and calcified fibrocartilage, and bone; however, transitions between zones are gradual and continuous. Furthermore, even at an ultrastructural level, there are no clearly-defined boundaries between the zones (6). This unique structure functionally distributes mechanical stress and enhances the bonding strength between soft and hard tissue (7). Despite recent advances in surgical techniques and satisfactory clinical outcomes (8-10), studies have shown that the structure of the TBI is not fully recovered to normal after rotator cuff repair but filled with poorly disorganized neo-fibrovascular scar tissue (11), including reduced continuity and orientation of the collagen fibers, scarce reconstruction of the fibrocartilage zones, and lack of calcium distribution (7, 12). This scar tissue eventually contributes to reduced mechanical strength, resulting in high re-tear rates of 27 - 94% (7, 12-14). Therefore, a new strategy is needed to regenerate the TBI of rotator cuffs with continuous gradient structures which exhibits distinct characteristics of the normal tissue.

The development of biomimetic scaffolds has emerged as a promising approach for regenerating the rotator cuff structure. Although several researchers reported the efficacy of biomimetic scaffolds on regeneration of TBI structure, the scaffolds they used had limitations in representing the complex structure of the TBI of rotator cuff. Most of the researchers used one homogenous layer scaffold composed of acellular dermal matrix (15) or ovine forestomach ECM (16), or a multilayer scaffold in which all the layers had the same matrix (16). More recently, some studies have reported multi-layer scaffolds with two or more different phases for tendon to bone interface regeneration (7). Fabrication techniques for multi-layer scaffolds involve several freeze-drying steps or further processing to assure an adequate adhesion of various layers. However, they often demonstrated instability at the interface between tendon to bone tissue (17-19). Therefore, it would be necessary to investigate the gradient scaffold fabricated as a single layer with a highly porous structure, without any discrete separations at the interfaces and the need for further processing to assure stable adhesion between different layers.

The scaffold should not only be able to mimic the unique structure of the TBI of rotator cuffs but also act as an artificial extracellular matrix (ECM) to provide the cells with mechanical support and physiochemical microenvironments (20). Some decellularized allogenic or xenogenic scaffolds are introduced for human patients using several tissues such as human dermal, porcine SIS, porcine urinary bladder, and porcine heart valves (21). However, most decellularized tissues

have been derived from animals or cadavers and there are some of some concerns about immunogenicity and pathogen transmission. Adipose tissue (AD) is the predominant source of ECM material in the human body. It is associated with minimal anti-host inflammation because of its homogeneity, even among different species. The ECM derived from AD has basic components of the TBI structure, including elastin, laminin, glycosaminoglycans (GAGs) and collagen. Especially, the collagen contained predominant proportion of the type I collagen (21) with a low level of antigenicity (22), which can regulate cell behaviors such as adhesion, proliferation, and survival (22). Thus, ECM made from AD could be a good material to fabricate scaffolds to regenerate the TBI of rotator cuffs. However, the ECM does not have sufficient calcium (23), a material that increases linearly from the tendon to the bone in normal TBI structure, which contributes to the mechanical strength of the rotator cuff (23, 24). Hydroxyapatite (HA) is a compositional and structural basic building block of original calcified ECM (25) with good osteoconductivity and osteoinductivity (26). Therefore, addition of HA gradient in the scaffold could compensate for the lack of calcium in an AD derived-ECM scaffold. For these reasons, the AD derived-ECM scaffold with an HA gradient (HA-G scaffold) could be a suitable material to mimic the structure of the TBI as a single layer with mechanical gradient and provide cells with a favorable microenvironment to regenerate the structure of the TBI.

Cells are essential elements for tissue engineering and produce



synergistic effects with scaffolds. The commonly employed cell populations include tenocytes, chondrocytes, osteocytes and mesenchymal stem cells (MSCs) (27, 28). Tenocytes, chondrocytes and osteocytes are crucial cell sources for recreating specific tissues of the TBI, yet these permanently differentiated cells have reduced metabolic activity and expression of specific lineage markers, such as tenogenic, chondrogenic, and osteogenic markers, during serial passage (20, 29, 30). However, MSCs have the potential to differentiate into preferred lineages including osteocytes, chondrocytes, and tenocytes (31, 32). Recently, bone marrow-derived MSCs (BM MSCs) and adipose tissue-derived MSCs (AD MSCs) are used with scaffolds to regenerate the structure of TBI (33-35); however, these MSCs have several disadvantage such as invasive techniques during harvesting (36), low collection efficiency (37), decreased ability with the age, and morbidities of donors and heterotopic matrix formation (38). Besides these MSCs, one of the promising candidates is umbilical cord derived MSCs (UC MSCs) which possess faster proliferation capacity, maintains higher survival rates despite many passages (39), are less affected by aging (40-42). In addition, UC MSCs could be obtained by non-invasive method at a relatively low cost because umbilical cord is medical waste after delivery. Moreover, UC MSCs have low immune rejection response because they exhibit high expression of major histocompatibility complex (MHC) class I and low expression of MHC class II suggesting clinically acceptable immunogenicity (43). Recently, several studies showed that UC MSCs contributed to the

healing process in tissue injuries such as degenerative muscle injury, hindlimb ischemia injury, and skin wound injury in vivo (44-46). This suggested that UC MSCs have healing capacity after musculoskeletal injury and could produce a synergistic effect with scaffolds when used in the regenerative engineering field.

Hence, the purpose of this study was to investigate the specific matrix formation by MSCs according to the HA gradient in ECM scaffold made from AD and effect of UC MSC seeded HA-G scaffolds on the regeneration of the TBI in a rotator cuff repair rat model. It was hypothesized that the HA-G scaffold made from AD promotes UC MSCs to form specific matrices similar to the TBI structure and that the UC MSC seeded HA-G scaffold could regenerate of the TBI of the rotator cuff with histological and biomechanical properties similar to the normal TBI of rotator cuffs.

## II. Materials and Methods

### 1. Scaffold fabrication

Human AD obtained by liposuction was washed several times with distilled water to remove the blood components. Crude ECM was isolated from the adipose tissue by homogenization, centrifugation, and rinsing. The ECMs were cast in a mold, frozen overnight  $-20^{\circ}\text{C}$ , and freeze-dried. For decellularization, the freeze-dried ECM scaffolds were treated with buffered 0.5% sodium dodecyl sulfate (SDS; Sigma, St. Louis, MO, USA) for 1 h at room temperature in a shaking water bath. The sheets were thoroughly rinsed with distilled water for 24 h at  $4^{\circ}\text{C}$  under shaking. The medium was replaced every 2 h with fresh distilled water. The decellularized ECM sheets were lyophilized in a freeze-dryer for at least 48 h.

To mimic the TBI, I prepared a scaffold consisting of gradient calcium by a calcium-phosphate dipping method. The decellularized ECM scaffolds were cross-linked in the presence of chondroitin sulfate (CS) (Tokyo Chemical Industry, Tokyo, Japan) using 1-ethyl-3(3-dimethyl aminopropyl) carbodiimide (EDC) and N-hydroxysuccinimide (NHS). The ECM was immersed in 40% v/v ethanol containing 50 mM 2-morpholinoethane sulfonic acid (MES) and incubated at room temperature for 30 min. Subsequently, the ECM was incubated with 40% v/v ethanol containing 50 mM MES and 2% w/v CS at room temperature for 4 h with 5 mg/mL EDC to yield an

ECM-CS composite at a ratio of 9:1. NHS was added to achieve an EDC:NHS ratio of 4:1. After the reaction, excess EDC and CS were rinsed from the matrix using 0.1M  $\text{Na}_2\text{HPO}_4$  for 1 h. ECM scaffolds were immersed in 500 mM calcium chloride dehydrate solution ( $\text{CaCl}_{22}\text{H}_2\text{O}$ ; Sigma-Aldrich) for 5 min and rinsed for 1 min in distilled water. Subsequently, the ECM scaffolds were immersed in 300 mM disodium hydrogen phosphate solution ( $\text{Na}_2\text{HPO}_4$ ; Duksan Pure Chemical, Ansan, Korea) for 5 min and rinsed for 1 min in distilled water. The HA-gradient ECM scaffolds were frozen overnight  $-20\text{ }^{\circ}\text{C}$ , followed by free-drying for 48-72 h. Both calcium and phosphate solutions contained 0.1 M potassium chloride (KCl; Sigma-Aldrich) to maintain ionic stability and were adjusted to pH 8.22. The Ca/P molar ratio of the precipitates at pH 8 exhibited a close stoichiometric composition (Ca/P51.67) of HA. After being sterilized by ethylene oxide gas, these scaffolds (thickness 2 ~ 3 mm, diameter ~10 mm) were used as the HA-G scaffold group.

## 2. The HA-G scaffold characterization

The pore size and the porosity were determined using an automated mercury porosimeter (Autopore IV 9500, Micromeritics, Norcross, GA, USA). The morphology of the HA-G scaffold was observed by scanning electron microscopy (SEM; S-4800 FE-SEM, Hitachi, Tokyo, Japan) at an accelerating voltage of 10 kV after platinum coating with a sputter coater (Emitech k575x; Quorum Technologies,

Wellington, UK). The HA-G scaffold was generally coated with CS and contained a gradually increasing calcium. The components of the scaffold were confirmed using an fourier transform infrared (FTIR) spectrophotometer. The FTIR spectrum was obtained in an attenuated total reflectance mode with a Nicolet 6700 FTIR spectrometer equipped with a diamond probe (Thermo Fisher Scientific, Waltham, MA, USA). The results from an average of 256 scans in spectral range between 1800 and 800  $\text{cm}^{-1}$  were obtained. The weight fraction of the HA in the different parts (tendon phase, cartilage phase and bone phase) of the HA-G scaffold was measured with a thermogravimetric analysis (TGA) apparatus (TG-DTA 2000SA; Bruker AXS, Billerica, MA, USA) upon heating from 25 °C to 800 °C at 10 °C/min under an N<sub>2</sub> atmosphere. For mechanical properties evaluation, the compressive strength of HA-G scaffold was measured using universal testing machine (TA.XT Express Connect, Texture Technologies Corp. Hamilton, MA) with a 5-Kgf load cell. The testing speed was 0.1 mm/s and pre-load intensity was 0.5 N. For evaluation DNA contents, DNA was isolated with a commercially available extraction kit (G-spin Total DNA Extraction Kit, iNtRON Biotechnology Inc, Korea). The total DNA content was measured by absorption at 260 nm on a spectrophotometer (NanoDrop 1000, Thermo Fisher Scientific, Wilmington, DE). All samples were normalized to the ECM sheet dry weight.

### 3. UC MSCs isolation and culture

This study was approved by the Institutional Ethical Review Board (IRB 06-2012-78) and was conducted in accordance with the approved guidelines. All patients from whom tissue specimens were collected provided informed consent. UCs (n = 3) were washed twice in demineralized phosphate-buffered saline (DPBS) and finely minced into 1 mm to 2 mm fragments using surgical scissors and scalpels. Cells were released by treating these fragments with 0.075% collagenase type I at 37 °C for 2 h with gentle agitation. After adding the same volume of DPBS, undigested tissues were removed using a 100 µm nylon sieve. Cells were collected by centrifugation, washed twice, resuspended in growth medium, i.e., low glucose DMEM (SH 30021.01, GE Healthcare Life Science) containing 10% inactivated fetal bovine serum (FBS) (SH 30919.03, Thermo Fisher Scientific) and 1% penicillin/streptomycin (LS 203-01, Welgene, Gyeongsan-si, Korea). They were plated into 100-mm tissue culture dishes at a density of  $1 \times 10^4$  cells/cm<sup>2</sup> for expansion at 37 °C in a humidified incubator with a 5 % CO<sub>2</sub> atmosphere for 3 - 4 days for the cells to adhere. The medium was replaced every three days and the cells were split at a ratio of 1:4 at 80 % confluence. UC MSCs at passage 10 were used for all experiments

### 4. Characterization of UC MSCs

When UC MSCs reached 80% confluence, cell morphology was observed under a microscope (CKX53 Olympus culture microscope; Olympus, Tokyo, Japan).

Cell viability of MSCs was determined by trypan blue exclusion. Cells were stained with trypan blue (0.4%) solution and the live and dead cells were counted using the hemocytometer. The percentages of cell viability of MSCs were calculated using the following formula: total number of live cells/total number of cells x 100 (%)

For flow-cytometry evaluation, harvested cells aliquoted at a concentration of  $5 \times 10^5$  cells/tube in supplemented with 2 % fetal bovine serum (FCS buffer) and stained with cell surface antibodies including positive markers (CD73, CD90 and CD105) and negative markers (CD11b, CD19, CD34, CD45, or HLA-DR) (BD Biosciences, San Jose, CA, USA) for 30 min at 4 °C in the dark. IgG1 isotype-FITC, IgG1 isotype-PE and IgG2a isotype-FITC were used as the isotype controls; IgG1 isotype-FITC for CD90, CD105 and CD11b, IgG1 isotype-PE for CD45, CD73, CD19, CD34, and IgG2a isotype for HLA-DR (BD Biosciences, San Jose, CA, USA). Then, the cells washed once with ice-cold DPBS and centrifuged at 500 g for 3 min, and fixed in 1% paraformaldehyde solution. 10,000 events were collected and analyzed the events using a Flow Cytometer FC500 (Beckman Coulter, Brea, CA, USA) with CXP Cytometer 2.3 software (Beckman Coulter, Brea, CA, USA).

Multipotent differentiation potential of UC MSCs was also

evaluated: tenogenic, chondrogenic, osteogenic and adipogenic differentiation.

For tenogenic differentiation, I made tensioned three-dimensional constructs. A 5 mL aliquot of Sylgard (Dow Corning, Midland, MI, USA) was added to 6-well plates (30006, SPL Life Sciences, Co., Ltd.). Two cotton thread sutures approximately 5 mm in length were pinned to the Sylgard surface of the dishes, 15 mm apart, using stainless steel minuten pins (Interfocus, Cambridge, UK). The dishes were sterilized by soaking in 70% ethanol for 1 h and then washed with DPBS twice. After air drying, the growth medium was added for 24 h. After removing pre-soaking media, the UC MSCs ( $5 \times 10^5$  cells/well) in 1 mL growth medium supplemented with 2 mg fibrinogen (F3879 Sigma-Aldrich), 1  $\mu$ L aminohexanoic acid (07260 Sigma-Aldrich), and 1  $\mu$ L aprotinin (10236624001 Roche, UK) were mixed with 0.5 U thrombin (Reyon Pharmaceutical, Weoul, Korea) per well. The UC MSCs were then layered on the culture dish, followed by incubation for 3 h at 37 °C, and addition of 3 mL growth medium supplemented with ascorbic acid 2-phosphate (250  $\mu$ M; Sigma-Aldrich) and proline (50  $\mu$ M; Sigma-Aldrich). Culture plates were incubated at 37 °C and 5% CO<sub>2</sub> for the duration of the experiment. Medium was changed every 3 days. After 7 days, the tissue was harvested and stained with picosirius red (PSR).

For chondrogenic differentiation, UC MSCs seeded at a density of  $2 \times 10^5$  cells/tube into the 15 mL polypropylene tube (Corning, NY,



USA) with differentiation medium (high-glucose Dulbecco's modified Eagle's medium (HG-DMEM; Hyclone, Logan, USA) with 10% FBS, 1% antibiotic-antimycotic solution, 0.1  $\mu$ M dexamethasone, 50  $\mu$ g/ml L-ascorbic acid 2-phosphate sesquimagnesium salt hydrate, 1X insulin-transferin-selenium-X, 40  $\mu$ g/ml L-proline, 5  $\mu$ g/ml linoleic acid, 100  $\mu$ g/ml sodium pyruvate (all reagents from Sigma Aldrich, US), and 10  $\mu$ g/ml transforming growth factor beta 1 (TGF $\beta$ -1; PeproTech, London, UK). The medium was changed every 3 days. After 14 day, the tissue was harvested and stained with Safranin-O/fast green (Saf-O).

For osteogenic differentiation, UC MSCs seeded at a density of  $0.75 \times 10^4$  cells/cm<sup>2</sup> into the 24-well plate with differentiation medium (high-glucose Dulbecco's modified Eagle's medium with 10% FBS, 1% antibiotic-antimycotic solution, 0.1  $\mu$ M dexamethasone, 50  $\mu$ g/ml L-ascorbic acid 2-phosphate sesquimagnesium salt hydrate, 10 mM  $\beta$ -glycerophosphate disodium salt hydrate (all reagents from Sigma Aldrich, US). The medium was changed every 3 days. After 21 days, the tissue was harvested and stained with Von Kossa.

For adipogenic differentiation, UC MSCs seeded at a density of  $0.75 \times 10^4$  cells/cm<sup>2</sup> into the 24-well plate with differentiation medium (high-glucose Dulbecco's modified Eagle's medium with 10% FBS, 1% antibiotic-antimycotic solution, 1  $\mu$ M dexamethasone, 60  $\mu$ M indomethacin, 500  $\mu$ M 3-isobutyl-1-methylxanthine, 5  $\mu$ g/ml insulin (all reagents from Sigma Aldrich, St. Louis, MO, US). The medium

was changed every 3 days. After 21 days, the tissue was harvested and stained with Oil red O (Sigma Aldrich, US).

## **5. UC MSCs seeding to the HA-G scaffold**

Prior to UC MSCs seeding, the HA-G scaffold was divided into four equal parts in fan-shape. The divided scaffolds placed into each well of a non-treated 24-well polystyrene plate (32024, SPL Life Sciences, Pocheon-si Korea) and the growth medium was added for two hours. The cell suspension (10  $\mu$ l,  $1 \times 10^5$  cells) was seeded onto the tendon phase of the scaffold for one hour. After the scaffold was inverted, 10  $\mu$ l of the cell suspension was also seeded onto the bone phase of the scaffold. After one hour, 1 ml of growth medium was added to each well (Figure 1). The cell seeded scaffolds were placed at 37 °C in a humidified incubator with a 5% CO<sub>2</sub> atmosphere for one day to allow the cells to adhere. The scaffold media was changed to saline after seven days before transplantation in the animal experiments.

## **6. Adhesion and proliferation of UC MSCs in the HA-G scaffold**

The adhesion efficiency of the UC MSCs to the HA-G scaffold was evaluated by counting the number of cells and by using a water-soluble tetrazolium salt (WST) assay. After transferring the

scaffolds to a new 24-well plate, the non-adherent cells left in the cell culture plates were collected in a trypsin/EDTA solution and the cell numbers were counted using a hemocytometer. The cell seeding efficiency was calculated as the number of adherent cells (total cells - non-adherent cells) divided by the total number of seeded cells. A WST assay kit (EZ3000, DAEILLAB SERVICE CO.LTD) was also used to determine the adhesion efficacy. At 24 h of culture, the cell-seeded scaffolds were rinsed with phosphate-buffered saline and incubated with 1.5 mL of 10% WST solution in the dark at 37 °C in a humidified incubator with a 5% CO<sub>2</sub> atmosphere for two hours. After gentle pipetting, 100 µL of the solution was transferred to a 96-well plate. The optical density was then measured at a wavelength of 450 nm using a microplate spectrophotometer (Power Wave XS; Bio-Tek Instruments, Winooski, VT, USA). To visualize the adherent live cells, a calcein-AM assay was used. Before seeding, the MSCs were stained with calcein-AM dye (C3099; Invitrogen, Carlsbad, CA, USA) solution. The cells were washed with D-PBS and were incubated with calcein-AM at 37°C for 30 min. The stained cells were washed twice with serum-free media and incubated with the scaffold at 37°C for 24 h. Last, the scaffold was carefully washed four times with serum-free media and the stained samples were placed on a microscope slide. The slide was observed under a fluorescence microscope (Leica DMI 4000B, Bensheim, Germany).

The proliferation kinetics of the UC MSCs in the scaffolds was determined using 4',6-diamidino-2-phenylindole (DAPI) staining (1,

3, 7, 14 and 21 days), SEM imaging (1, 3, 7, and 14 days), and the WST assay (1, 3, 7, 14, and 21 days). The cells were fixed with 4% paraformaldehyde, stained with DAPI, and visualized under a fluorescence microscope. The DAPI stained cells were counted for quantification of proliferated cells. Moreover, the cells at tendon, cartilage and bone phases evaluated separately at 21 days to analyze the proliferation variation according to each site of the HA-G scaffold. The morphology of the cells attached to the scaffold was examined by SEM. The cell-seeded scaffold constructs were fixed in 2.5% glutaraldehyde for 30 min. After cell fixation, they were dehydrated through a graded series of ethanol solutions (from 50 to 100% in increments of 10%) for 10 min each and freeze-dried under vacuum for two days. The samples were coated with platinum by sputter-coating and then observed by SEM at an accelerating voltage of 5 kV. Last, a WST assay was performed according to the above-mentioned protocol and the values for 3, 7, 14, and 21 days were normalized to day 1.

## **7. Matrix formation of tendon, cartilage, and bone by UC MSCs**

The HA-G scaffold and the UC MSC-seeded HA-G scaffold (UC MSC + HA-G scaffold) were harvested at 4 weeks. All specimens were immediately fixed in 4% (w/v) paraformaldehyde (PFA;

Merck, Germany) for 24 hours, embedded in paraffin, and sectioned at a thickness of 4  $\mu\text{m}$ . The slides were randomly selected and stained with hemotoxylin and eosin (HE) to analyze the general morphologic changes and ECM of the scaffolds, Masson's Trichrome (MT), Saf-O, and Von-kossa. The stained slides were observed by light microscopy (U-TVO 63XC; Olympus Corp., Tokyo, Japan).

The HE stained slides were used to analyze the general morphologic changes and ECM of the scaffolds. The MT stained slides were used to evaluate newly formed collagen, which is the main component of the tendon region and a tenogenic differentiation marker of UC MSCs. The Saf-O stained slides were used to evaluate the deposition of glycosaminoglycan (GAG), which is the main component of the cartilage region and a chondrogenic differentiation marker of UC MSCs.

To evaluate type 2 collagen, I performed immunohistochemical analysis (IHC). Type 2 collagen was also used as a chondrogenic differentiation marker of the UC MSCs. Randomly selected slides were incubated in trisodium citrate buffer (pH = 6.0) for 15 mins at 95 °C. After blocking with 3% hydrogen peroxide for 10 min and superbloc (AAA500; ScyTek, Logan, Utah, USA) at room temperature, the sections were incubated with antibody to type 2 collagen (1:100, ab34712, Abcam, Cambridge, UK) at room temperature for 2 hours. The slides were rinsed with deionized water and then PBS, followed by 30 min of incubation with the secondary

antibody solution (K4002, Dako: Carpinteria, CA, USA). After washes with PBS, a 3,3'-diaminobenzidine (DAB) (C09-12, GBI Labs, Bothell, Washington, USA) working solution was added and incubated at room temperature for 1 min. The slides were then lightly counterstained with hematoxylin.

Last, the Von-kossa stained slides were used to evaluate the deposition of calcium, which is the main component of the bone region and an osteogenic differentiation marker of UC MSCs.

Areas of collagen, GAG, type 2 collagen, and calcium from each slide were quantified separately according to the tendon, cartilage and bone phases using ImageJ software with an NII plugin (National Institutes of Health, MD, USA). I also evaluated the areas using semi-quantitative evaluation method using a 0-3 grading scale (47).

## 8. In vivo study design

This study was approved by the Institutional Animal Studies Committee (IACUC-2016-0030). Adult male Sprague-Dawley rats (121, 12 weeks old, 300 – 350g) were used and the rats were divided into six groups 1) the defect, 2) the repair, 3) the UC MSC, 4) the HA-G scaffold, 5) the UC MSC + HA-G scaffold, and 6) the control. Rats from each group were euthanized at 4 and 8 weeks for histologic evaluation (n = 4) and 4 and 8 weeks for biomechanical evaluation (n=12) after surgery. Additionally, one more animal was put in the

HA-G scaffold group and harvested the animal at day 0 to ensure that the scaffold was located in the right place between the supraspinatus tendon (SST) and the bone after the operation.

## 9. Surgical procedures

Anesthesia was induced using zoletil and rompun (30 mg/kg + 10 mg/kg). Bilateral shoulders were operated on in all cases. A 2 cm skin incision was made directly over the anterolateral border of the acromion. After the SST was exposed by detaching the trapezius and deltoid muscle from the acromion, the SST was detached sharply from its insertion site. In detail, the distal site of transected SST was removed to remove TBI structure by 1mm. In addition, to prevent the tendon from naturally attaching to the bone, the supraspinatus was completely separated from, infraspinatus, and subscapularis to allow SST to retract by the force of supraspinatus muscle. The residual TBI structure on the greater tuberosity was removed entirely using a bur until bleeding. When performed repairs, before detaching the SST, 5-0 Ethibond (W6890, Ethicon, Cincinnati, OH, USA) was applied transversely 1mm below the musculotendinous junction to prevent tearing of the tendon due to the pulling force of the repairing thread. Directly above the Ethibond in transverse, new two Ethibond were passed and detached the SST from the bone. The residual TBI structure on the greater tuberosity was removed. Two 0.6-mm drill holes were crisscrossed in an anterior-posterior orientation through the

proximal part of the humerus. Two Ethibond was passed through a drilled hole without or with HA-G scaffold or UC MSC + HA-G scaffolds between the tendon and the bone at SST removed site and tied in a crisscross shape. After repair, the deltoid and trapezius muscle incisions were sutured with 4-0 Vicryl suture (W9074, Ethicon) and the skin was also sutured with black silk (SK4345, AILee, Busa, Korea) (Figure 2). In the defect group, the SST was detached, but no further surgical procedure was performed. In the repair group, the SST underwent repair, but no other procedure was performed. In the UC MSC group, the SST underwent repair and the repair site was injected with UC MSCs ( $2 \times 10^5$  cells per 20  $\mu$ L saline). In the HA-G scaffold group, the SST underwent repair with HA-G scaffolds. In the UC MSC + HA-G scaffold group, the SST underwent repair with UC MSC ( $2 \times 10^5$ ) seeded HA-G scaffolds. In the control group, the SST was exposed, but no further surgical procedure was performed (the sham control). After surgery, the animals were allowed free cage activity.

## 10. Histological evaluation

At day 0, 4, and 8 weeks, the rats were sacrificed in a carbon dioxide chamber. The SST of the rats was harvested with the humeral head and were immediately fixed in 4% (w/v) PFA for 24 hours and underwent decalcification in 10% ethylenediaminetetraacetic acid (EDTA) (Sigma-Aldrich) for 8 days. After decalcification, the tissues



were dehydrated through an increasing ethanol gradient, defatted in chloroform, and embedded in paraffin blocks. The tissues were sagittally positioned and carefully trimmed until I found the middle area of the repair site by using the suture marker. When I found the appropriate site, I serially cut 20 slides with 4  $\mu\text{m}$  thickness. Then, I randomly used two slides for each stain.

A randomly selected slide was stained with HE and analyzed by light microscopy (U-TVO 63XC; Olympus Corp.). To determine the regeneration of the TBI, each slide was evaluated with the semi-quantitative scoring system reported by Watkins et al. (48) and modified by Ide et al. (49). There were 8 parameters in the system: fiber arrangement, fiber large diameter, cellularity, vascularity, fibrocartilage cells, tidemark, continuity and bone ingrowth. Each slide is assigned a score from 1 (most severely damaged TBI) to 4 (normal TBI) for each parameter. The total regeneration score for a given slide could vary between 8 (most severely damaged TBI) and 32 (normal TBI).

The slides were stained with PSR and analyzed for collagen deposition and maturation at the tendon zone. Collagen organization was quantified using circularly polarized light microscopy at x200 magnification. The polarization plane was rotated until maximum brightness was obtained. After obtaining the photo, the image underwent 8-bit digitization and Collagen organization was measured as intense white areas of brightly diffracted light on gray scale (black,

0; white, 255) using ImageJ software with installed NII plugin (National Institutes of Health, MD, USA). Higher gray scale indicated more organized and mature collagen (50).

To evaluate the cartilage formation at the cartilage zone of the TBI, the slides were stained with Saf-O and type 2 collagen (IHC method above for scaffold staining). In the Saf-O stained slide, the total area of metachromasia at the defect site was determined by measuring the area of cartilage-related GAG using Image J (38, 51). Moreover, a tidemark at the cartilage zone indicated that a calcified fibrocartilage region and an uncalcified fibrocartilage region were formed separately (52). Thus, the length of the tidemarks in HE stained slides was measured by Image J software. The GAG area and the length of the tidemark were normalized by those in the control group.

## **11. Biomechanical evaluation**

For biomechanical testing, I harvested the supraspinatus tendon with the humeral head and carefully removed the muscles to leave only the tendon. The harvested tissues were wrapped in saline-soaked gauze and kept at -80 °C. Before testing, the tissues were thawed with saline wet gauze at room temperature for 24 hours and the tissues were kept moist with saline during all of the tests. The distal part of the humeral bone was vertically embedded in an aluminum tube filled with polymethylmethacrylate (PMMA) in the custom-designed lower

jig of a testing system. The proximal end of the tendon was compressed with sandpaper, gauge, and rubber to prevent slippage and to reduce damage to the specimens. The complex was clamped vertically in the custom-designed upper jig. Testing was performed with the shoulders at 90° of abduction with a material testing system (H5K5, Tinius Olsen, England, UK) (53, 54) (Figure 13A). All specimens were initially preloaded to 0.2 N and preconditioned for five cycles under 5% of strain at a rate of 0.1 mm/s. Then, these specimens were loaded to failure in tension at a constant rate of 0.1 mm/s. Slippage of the tendon was inspected visually. The cross-sectional area of the supraspinatus tendon was measured at the TBI. The load-displacement curve recorded during tests and the ultimate failure load, stiffness and ultimate stress were calculated. During the test, the anatomic location of the failure in one of three locations, tendon, TBI, or bone, was also recorded to analyze the failure mode.

## 12. UC MSCs trafficking

Anti-human mitochondrial antibody (1:200; ab92824, Abcam, Cambridge, UK) was used to detect the human UC MSCs in the UC MSC-HA-G scaffold after implantation at 4 and 8 weeks. After dewaxing and rehydration, the slides were incubated with pepsin solution Digest-All (Invitrogen, Carlsbad, CA, USA) for 20 mins at room temperature for anti-human mitochondrial IHC. After blocking

with 3% hydrogen peroxide and superblock (AAA500, ScyTek, Logan, Utah) for 10 min at room temperature, the sections were incubated with primary antibody solution overnight at 4 °C. The sections were rinsed with deionized water and then PBS, followed by 30 min of incubation with a secondary antibody solution (K4002, Dako, Glostrup, Denmark). After washing, DAB working solution was added and incubated at room temperature for 30 seconds. These slides were then lightly counterstained with hematoxylin. The slides were observed by light microscopy at x400 magnification. The anti-human mitochondrial antibody-positive cells were counted per area and the mean number was used in image J (55).

### **13. Statistical analysis**

All data are shown as the mean  $\pm$  SD. The continuous numeric data were analyzed with one-way analysis of variance (ANOVA) with post-hoc analysis by Bonferroni multiple comparison tests. The cell trafficking data were analyzed by Mann-Whitney analysis. All statistical analyses were performed with SPSS software version 23 (IBM, Chicago, USA). Differences of  $p < 0.05$  were considered statistically significant.

### III. Results

#### 1. Characterization of HA-G scaffolds

The scaffold had a typical highly porous microstructure (decellularized ECM scaffold mean pore size: 150  $\mu\text{m}$ , porosity: 89%). Macroscopic appearance and SEM images of the HA-G scaffold are shown in Figure 3A. The HA-G scaffold had similar microstructure and high interconnectivity (HA-G scaffold mean pore size: 100-150  $\mu\text{m}$ , porosity: 91%) and the numbers of HA particles were progressively increased from the tendon to the bone (Figure 3A). The FTIR spectrum of the scaffold is displayed in Figure 3B. The scaffold had two major amide absorption bands of collagen at 1628 - 1647 (1645)  $\text{cm}^{-1}$  and 1539 - 1560 (1542)  $\text{cm}^{-1}$ , corresponding to amide I and II, respectively. The results were comparable to the spectra of collagen from other sources (22). Comparable absorbance bands for CS were observed at 1411 - 1413 ( $\text{COO}^-$ , 1419). Sugar groups were observed in the range of 970 - 1120 (984, 1051, and 1119)  $\text{cm}^{-1}$ . However, it was difficult to distinguish the amide III (1232 - 1243  $\text{cm}^{-1}$ ) absorption bands of collagen and the  $\text{SO}_4^{2-}$  (1225 - 1258  $\text{cm}^{-1}$ ) absorption bands of CS because of overlap. The vibrational bands of phosphate and carbonate caused by HA were visible at 1020 and 871  $\text{cm}^{-1}$ , respectively (Figure 3B). TGA comparatively showed the HA content of the HA-G scaffold (Figure 3C). The first weight loss observed between 25  $^{\circ}\text{C}$  and 100  $^{\circ}\text{C}$  corresponded to the removal of water in each composite, whereas the second weight loss occurred at 250 -

550 °C, associated with the loss of organic content. The collagen/HA (organic/inorganic) mass ratios of three parts in the HA-G scaffold were 87/13 (tendon phase), 82/18 (cartilage phase), and 63/37 (bone phase), respectively. Compressive strength of three parts in the HA-G scaffold was analyzed  $1.26 \pm 0.04$  MPa (tendon phase),  $1.9 \pm 0.4$  MPa (cartilage phase), and  $2.9 \pm 0.7$  MPa (bone phase), respectively (Figure 3D). DNA contents in AD and decellularized ECM scaffold were analyzed  $530 \pm 80$  ng/mg and  $76 \pm 14$  ng/mg, respectively.

## **2. Characterization of UC MSCs**

UC MSCs showed fibroblast-like morphology and viability of the cells were 100% (Figure 4A and 4B). In flow-cytometry results, the cells were positive for CD73, CD90 and CD105 and were negative for CD11b, CD19, CD34, CD45 and HLA-DR (Figure 4C). In multipotent differentiation evaluation, the cells was differentiated into the four types of cells such as tenocyte, chondrocytes, osteoblasts and adipocytes respectively (Figure 4D)

## **3. Adhesion, infiltration, and proliferation of UC MSCs in the HA-G scaffold.**

After 24 h, calcein-AM stained UC MSCs (green signal) were detected on the surface of the HA-G scaffold (Figure 5A). The

adhesion rate of the UC MSCs to the HA-G scaffold was  $98.0 \pm 0.9\%$  using a counting method and  $97 \pm 2\%$  by WST analysis (Figure 5B). After seeding, UC MSCs remained only on the superficial surface (bone and tendon phases) of the HA-G scaffold at 1 day and then progressively migrated toward the cartilage phase (a middle region) at 3 days. At 7 and 14 days, the UC MSCs were observed inside and distributed homogeneously throughout the HA-G scaffold (Figure 6A and 6B). The WST results showed that the proliferation of UC MSCs slowly increased ( $1.8 \pm 0.1$ -fold) until 7 days and then sharply increased at 14 and 21 days ( $3.8 \pm 0.6$  and  $6 \pm 2$ -fold, respectively; Figure 6C). The DAPI stained cells counting results showed that there was no significantly different proliferation according to the tendon and cartilage and bone phases at 21 days (Figure 6D).

#### **4. Histological evaluation of differentiated UC MSCs in HA-G scaffold**

Twenty-eight days after seeding UC MSCs in the HA-G scaffold, the HE stained tissues showed that more of the empty site of the scaffold was filled by ECM in the UC MSC + HA-G scaffold than in the HA-G scaffold (Figure 7A). The amount of newly formed collagen significantly increased by 2.89-fold in the UC MSC + HA-G scaffold compared to the HA-G scaffold at the tendon phase ( $p < 0.05$ ) (Figure 7B and 7F). The GAG and type 2 collagen scores

significantly increased by 6.93- and 9.96-fold in the UC MSC + HA-G scaffold compared to the HA-G scaffold at the cartilage phase respectively ( $p < 0.05$ ) (Figure 7C, 7G, and 7D, 7H respectively). The area of calcification significantly increased by 5.39-fold in the UC MSCs + HA-G scaffold compared to the HA-G scaffold at the bone phase ( $p < 0.05$ ) (Figure 7E and 7I). When compared within the UC MSCs + HA-G scaffold, collagen was the most common on the tendon phase, GAG and type 2 collagen on the cartilage phase, and calcium on the bone phase respectively.

## 5. Histological evaluation of regenerated tendon

I ensured that the inserted scaffold settled into the right place between the tendon and the bone at day 0 (Figure 8A). After 4 weeks, the total regeneration score was significantly higher in UC MSC + HA-G scaffold group ( $16.8 \pm 0.5$ ), compared to the defect group, ( $13.0 \pm 0.5$ ) ( $p < 0.05$ ). However, there was no significant difference among the repair operated groups (repair,  $16.9 \pm 0.8$ ; UC MSC,  $16.9 \pm 0.6$ ; and HA-G scaffold group,  $15.5 \pm 0.5$ ). After 8 weeks, the total regeneration score was significantly higher in the UC MSC + HA-G scaffold group, ( $22 \pm 1$ ) than in the defect group ( $15.1 \pm 0.5$ ), the repair group, ( $18 \pm 1$ ), and the UC MSC group, ( $17.8 \pm 0.7$ ) ( $p < 0.05$ ). In detail, fiber arrangement and fibrocartilage cells were significantly improved in the UC MSC + HA-G scaffold group compared to the defect group while there was no significantly



difference among other groups (Figure 8B and 8C). Additionally, in the detailed parameters of the regeneration scores, the bone ingrowth was not significantly different between the UC MSCs + HA-G scaffold group and that of other groups at both 4 and 8 weeks (Figure 9). There was no significant immune response against scaffolds and MSCs.

The collagen organization scores were higher in the UC MSC + HA-G scaffold group ( $80 \pm 20$ ) compared that of the defect, the repair, the UC MSC, and the HA-G scaffold groups ( $35 \pm 8$ ,  $50 \pm 20$ ,  $50 \pm 10$  and  $50 \pm 20$ , respectively) at 8 weeks. However, only the values in the defect group and the UC MSC + HA-G scaffold group were significantly different ( $p < 0.05$ ). Moreover, the collagen organization score in the UC MSC + HA-G scaffold group was comparable to that of the control group ( $85 \pm 8$ ) (Figure 10 ).

For cartilage formation, after 4 weeks, the area of metachromasia was significantly higher in the UC MSC + HA-G scaffold group ( $60 \pm 40$ ) compared to the other operated groups (the defect,  $0.00 \pm 0.00$ ; the repair;  $16 \pm 9$ ; the UC MSC,  $14 \pm 7$ ; and the HA-G scaffold,  $0.00 \pm 0.00$ ;  $p < 0.05$ ). Moreover, the area of metachromasia in the UC MSC + HA-G scaffold group was comparable to that of the control group ( $92 \pm 9$ ) at 4 weeks. After 8 weeks, the areas were significantly higher in the HA-G scaffold and UC MSC + HA-G scaffold groups ( $60 \pm 25$  and  $66 \pm 20$ , respectively) than those in the defect, and the repair, and the UC MSC groups ( $0.00 \pm 0.00$ ,  $30 \pm 10$ ,

and  $30 \pm 20$ , respectively) ( $p < 0.05$ ). Moreover, the area of metachromasia in the HA-G scaffold and the UC MSC + HA-G scaffold groups was comparable to the control group ( $113 \pm 5$ ) ( $p < 0.05$ ). The area of type 2 collagen also had a similar pattern as the area of metachromasia (Figure 11).

Tidemarks were not seen in any operated groups at 4 weeks. It became longer in the HA-G scaffold ( $11 \pm 7\%$ ) and the UC MSC + HA-G scaffold group ( $14 \pm 9\%$ ), whereas the tidemark was not observed in the defect, the repair, or the UC MSC groups at 8 weeks (Figure 12).

## 6. Biomechanical properties of regenerated tendons

Failure of the TBI occurred only in 8.33% of the HA-G scaffold group and in 16.67% of the UC MSC + HA-G scaffold group, whereas failure at the TBI site occurred in 66.67% of the defect group and 41.67% of the repair group at 4 weeks. After 8 weeks, the TBI failure rate was reduced overall in all groups. TBI failures occurred only in 16.67% of the defect group and 8.33% of the UC MSC + HA-G scaffold group (Figure 13B).

The cross-sectional area of the TBI significantly increased in all repair operated groups and there was no significant difference between the repair operated groups at 4 and 8 weeks (Figure 13C).

The ultimate failure loads were significantly higher in the UC MSC

+ HA-G scaffold group at 4 and 8 weeks ( $21 \pm 1$  N and  $23.0 \pm 0.7$  N, respectively) than those in the defect group ( $10.8 \pm 0.8$  N and  $16.1 \pm 0.8$  N, respectively), and the repair group,  $16.2 \pm 0.8$  N and  $19.8 \pm 0.5$  N, respectively) ( $p < 0.05$ ). The ultimate failure loads in the UC MSC + HA-G scaffold group were comparable to those of the control group ( $24.8 \pm 0.7$  N and  $23.8 \pm 0.9$  N, respectively) (Figure 13D).

At 4 weeks, stiffness was significantly higher in the UC MSC + HA-G scaffold group ( $6.8 \pm 0.6$  N/mm) than in the defect group ( $2.0 \pm 0.3$  N/mm) ( $p < 0.05$ ). The stiffness in the UC MSC + HA-G scaffold was comparable to that of the control group ( $7.8 \pm 0.8$  N/mm) ( $p < 0.05$ ). After 8 weeks, the stiffness was significantly higher in the UC MSC + HA-G scaffold group ( $7.2 \pm 0.2$  N/mm) compared to the defect ( $4.1 \pm 0.3$  N/mm), and the repair group ( $5.3 \pm 0.2$  N/mm) ( $p < 0.05$ ) (Figure 13E).

The ultimate stress was not significantly different between the UC MSC + HA-G scaffold group and the other repair operated groups at 4 and 8 weeks (Figure 13F). Thus, the UC MSC + HA-G scaffold group had an enhanced resistance to the tensile stress of the rotator cuff tendon, but the force per area of the tendon was still lower compared to the control group.

## 7. Human cell tracking

At 4 weeks, the mean number of anti-human mitochondrial

antibody-positive cells per area was  $200 \pm 100$  cells/mm<sup>2</sup>. At 8 weeks, the mean number significantly decreased 5.68% to  $13 \pm 2$  cells/mm<sup>2</sup>, compared to 4 weeks ( $p < 0.001$ ) (Figure 14).

## IV. Discussion

The most important findings of this study were 1) an HA-G scaffold had progressively increasing numbers of HA particles from the tendon to the bone phases similar to the intact TBI structure, and the UC MSCs highly adhered to and proliferated in the HA-G scaffold; 2) after seeding the UC MSCs, specific matrices, such as collagen, GAG, and calcium, were synthesized on the tendon phase, the cartilage phase, and the bone phase, respective to the gradient of the HA particles; 3) in the animal experiment, the UC MSCs + HA-G scaffold group had highly regenerated TBI structure by improving collagen organization by 52% at 8 weeks and cartilage formation by 262.96% and 145.13% compared to the repair group at both 4 and 8 weeks, respectively; 4) compared to the repair group, UC MSC + HA-G scaffold group had an enhanced ultimate tensile strength shown by increased ultimate failure loads of 30.71% and 16.08% at 4 and 8 weeks, respectively. The value at 4 weeks was comparable to that of normal tissue. Taken together, these results suggested that the gradient environment of the HA-G scaffold induced the UC MSCs to form specific matrices similar to the TBI according to the HA gradient and the UC MSC-seeded HA-G scaffold improved the regeneration of the TBI of the rotator cuff histologically and biomechanically.

The scaffold, in this study, had a highly porous ECM matrix with high interconnectivity. High porosity and interconnection significantly

influenced cell behavior, such as adhesion, infiltration, and migration (56), as well as the transport of oxygen, nutrients, and waste exchange (57). Moreover, the scaffold contained CS components, a major component of cartilage, and the progressive formation of HA, a basic component of bone. Cross-links between collagen and CS in the scaffold improved mechanical stability and offered a favorable environment for cells (58). Moreover, HA enhances not only the mechanical properties but also the bioactivity of the scaffold by providing a source of calcium and phosphate ions (59). In the fabricated scaffold in this study, UC MSCs had a high capacity for adhesion at 98.06%, as well as infiltration to the middle by 7 days, and was evenly distributed in the scaffold. Moreover, they proliferated by 3.84-fold at 14 days and 5.49-fold at 21 days. These proliferation rates were almost similar to commonly used engineered collagen scaffolds (26). These results indicate that an AD-derived ECM scaffold with HA gradient components was successfully fabricated and that the scaffold had good biocompatibility, supporting cellular adhesion, migration, and proliferation ability.

After seeding with the UC MSCs, the HA-G scaffold formed specific matrices at specific sites according to the HA density. The collagen matrix increased in the tendon phase, cartilage-related GAG and type 2 collagen matrix accumulated in the middle, and the calcium deposition increased in the bone phase of the HA-G scaffold. These results explained by the matrix elasticity of MSCs. MSCs have a specific lineage and synthesize a specific matrix via the matrix

physical microenvironment (60). Mineral components increase mechanical properties of a scaffold. Therefore, when the gradient calcium phosphate content also induced a gradient increase in the stiffness of a scaffold (7). It is proven that the elastic modulus increased according to the HA density in an adipose tissue-derived ECM scaffold by a dipping method in the previous study (59). Therefore, soft matrices that mimic tendons are tenogenic, stiffer matrices that mimic cartilage are chondrogenic, and comparatively rigid matrices that mimic bone are osteogenic according to the HA density in an HA-G scaffold. Moreover, CS coating, another base of the HA gradient scaffold, might also have a good impact on cartilage formation because CS not only affects cellular behaviors, including adhesion, migration, and differentiation but also promotes chondrogenesis, and induces the extensive deposition of proteoglycan and gene expression of type II collagen/type I collagen of MSCs (61). In addition, bioactivity of HA, well-known for its good osteoconductivity and osteoinductivity, could influence osteogenesis at the bone phase. Therefore, even in the absence of any other soluble differentiation factors, one-layer scaffold could elicit continuous specific matrix synthesis from a single MSC at once to form a continuous transitional structure of the TBI according to the HA density.

Clinically, fibrovascular scar tissue causes a high re-tear rate therefore, is the primary complication after rotator cuff repair surgery (62) and mainly occurs in the early-postoperative period at the repair site. Hence, facilitating the mean time for tissue regeneration is most

critical for the success of the operation. Recently, some researchers have tried to restore the scar tissue to its previous normal TBI structure using scaffolds in animal models (15, 16, 33). Li et al. showed a two-layer scaffold composed of poly-L-lactide (PLLA) and PLLA with an HA (nHA-PLLA) mimicking TBI structure: PLLA represents tendon and uncalcified fibrocartilage and nHA-PLLA represents calcified fibrocartilage and bone. The biphasic scaffold represented the unique TBI structure in more detail with increased collagen organization and improved metachromasia compared to a one-layer scaffold at 8 weeks. Despite the positive result, the scaffold had limitations in that it was composed of two separated layers and implantation of the PLLA material had a risk of inducing a fibrovascular response when used in the clinic (63, 64). In this study, the UC MSC + HA-G scaffold improved the structure of the TBI, such as collagen organization and fibrocartilage formation, without any further immune response. Especially, fibrocartilage was rapidly recovered and matures, instead of forming fibrovascular tissue at 4 weeks. These results derived from the gradient structure of a scaffold that well represented the gradient matrix of the TBI and the UC MSC, which synthesized specific matrices according to the specific region in relatively early healing phase (59). While histological findings improved until 8 weeks, most of the implanted UC MSCs disappeared by that time. Currently, beneficial effects of MSCs are reported to come from the paracrine mechanism: secretion of cytokines/growth factors that recruit, proliferate, and induce differentiation of tissue



specific progenitor cells to synthesis specific matrix (65). Additionally, MSCs could also regulate local inflammatory environment by modulating macrophage recruitment or polarization to M2 phenotype reducing inflammation and the presence of inflammatory cells (66). Therefore, although the implanted UC MSCs disappeared over time, the influenced local environment by MSCs could still affect to regenerate structure of damaged TBI at 8 weeks. Of course, more research is needed to explain this biologic process of paracrine effects of MSCs.

After injuries, the regenerated tissue became mechanically weakened because the strong normal structure of the TBI was replaced by weaker fibrous scar tissue (67-69). Previous studies showed that scaffold implantation improved some of the biomechanical properties of surgically repaired models and structural properties of the TBI. However, the ultimate failure load was still lower and failure of the TBI was still higher than those of the normal tissue even after 12 weeks (70, 71). In this study, the failure of the TBI in the UC MSC + HA-G scaffold group was only 16.67%, whereas it was 41.66% at 4 weeks in the repair group. Moreover, the ultimate failure load and stiffness in the UC MSC + HA-G scaffold group were significantly higher than that of the repair group at both 4 and 8 weeks. Specifically, the values of the ultimate failure load and stiffness at 4 weeks were 92.24% and 94.56% of 8 weeks; and 85.52% and 87.01% of the normal group respectively. These results showed that most of the mechanical properties of the TBI in the UC MSC + HA-G

scaffold recovered at early stage and were similar to the normal TBI. The biomechanical results were corroborated by the improved histologic results observed in this study. The tensile strength of the rotator cuff is derived from well-organized collagen fibers (72, 73) and the unique gradient structure of the TBI structure (7). Thus, it is suggested that the UC MSC-seeded HA-G scaffold promoted the recovery of the unique gradient structure of the TBI without disorganized fibrous scar tissue. The recovered structure would finally induce the functional recovery of the TBI though well-distributed tensile stress (7). Moreover, the earlier recovery of the UC + HA-G scaffold could prevent early tendon re-tears and could contribute to healing in later phases, which could lead to successful surgical outcomes (74).

There were several limitations to the study. First, an acute surgical repair model was used, which might not reflect chronic rotator cuff disease treated with surgery. However, an acute rotator cuff repair model has been widely used for the study of the regeneration of rotator cuffs after repair (75-77). Second, the calcium deposition by *in vivo* histological evaluation owing to the decalcification procedure during the preconditioning process of the specimens could not be quantified. Third, there is no widely accepted grading system for TBI regeneration. In this study, I used the grading system proposed by Ide et al. While this system has been used in a few studies, a specific grading system for the evaluation of TBI regeneration is needed. Forth, this study did not explain the mechanism of regeneration of

TBI structure. Although the regeneration might have occurred due to direct differentiation of UC MSCs and paracrine effects by UC MSCs, it is difficult to explain which pathways were involved in differentiation of MSCs into tenocytes, chondrocytes and osteocytes in the HA-G scaffold and which growth factors or cytokines secreted by MSCs influenced resident cells at the injury site. Thus, further study is needed to describe the healing mechanism of TBI of rotator cuff.

## V. Conclusion

HA-G scaffold made from AD induced UC MSCs to form tendon, cartilage and bone matrices similar to the TBI structure according to the HA density. Furthermore, UC MSC-seeded HA-G scaffold regenerated the TBI of the rotator cuff in a rat repair model in terms of histological and biomechanical properties similar to the normal TBI.

## VI. References

1. Chard MD, Hazleman R, Hazleman BL, King RH, Reiss BB. Shoulder disorders in the elderly: a community survey. *Arthritis Rheum.* 1991;34(6):766-9.
2. Gomoll AH, Katz JN, Warner JJP, Millett PJ. Rotator cuff disorders - Recognition and management among patients with shoulder pain. *Arthritis Rheum-Us.* 2004;50(12):3751-61.
3. Hermans J, Luime JJ, Meuffels DE, Reijman M, Simel DL, Bierma-Zeinstra SMA. Does This Patient With Shoulder Pain Have Rotator Cuff Disease? The Rational Clinical Examination Systematic Review. *Jama-J Am Med Assoc.* 2013;310(8):837-47.
4. Colvin AC, Egorova N, Harrison AK, Moskowitz A, Flatow EL. National Trends in Rotator Cuff Repair. *Journal of Bone and Joint Surgery-American Volume.* 2012;94a(3):227-33.
5. Aurora A, McCarron J, Iannotti JP, Derwin K. Commercially available extracellular matrix materials for rotator cuff repairs: State of the art and future trends. *J Shoulder Elb Surg.* 2007;16(5):171s-8s.
6. Kanazawa T, Gotoh M, Ohta K, Honda H, Ohzono H, Shimokobe H, et al. Histomorphometric and ultrastructural analysis of the tendon-bone interface after rotator cuff repair in a rat model. *Sci Rep.* 2016;6:33800.
7. Li XX, Cheng RY, Sun ZY, Su W, Pan GQ, Zhao S, et al.

Flexible bipolar nanofibrous membranes for improving gradient microstructure in tendon-to-bone healing. *Acta Biomaterialia*. 2017;61:204-16.

8. Galatz LM, Ball CM, Teefey SA, Middleton WD, Yamaguchi K. The outcome and repair integrity of completely arthroscopically repaired large and massive rotator cuff tears. *J Bone Joint Surg Am*. 2004;86-A(2):219-24.

9. Gulotta LV, Nho SJ, Dodson CC, Adler RS, Altchek DW, MacGillivray JD, et al. Prospective evaluation of arthroscopic rotator cuff repairs at 5 years: part I-Functional outcomes and radiographic healing rates. 2011;20(6):934-40.

10. Choi S, Kim MK, Kim GM, Roh Y-H, Hwang IK, Kang HJ, et al. Factors associated with clinical and structural outcomes after arthroscopic rotator cuff repair with a suture bridge technique in medium, large, and massive tears. 2014;23(11):1675-81.

11. Sharma P, Maffulli N. Biology of tendon injury: healing, modeling and remodeling. *J Musculoskelet Neuronal Interact*. 2006;6(2):181-90.

12. Eriskin C, Kalyon DM, Wang HJ. Functionally graded electrospun polycaprolactone and beta-tricalcium phosphate nanocomposites for tissue engineering applications. *Biomaterials*. 2008;29(30):4065-73.

13. Galatz LM, Ball CM, Teefey SA, Middleton WD, Yamaguchi

K. The outcome and repair integrity of completely arthroscopically repaired large and massive rotator cuff tears. *Journal of Bone and Joint Surgery-American Volume*. 2004;86a(2):219-24.

14. Sugaya H, Maeda K, Matsuki K, Moriishi J. Functional and structural outcome after arthroscopic full-thickness rotator cuff repair: Single-row versus dual-row fixation. *Arthroscopy*. 2005;21(11):1307-16.

15. Ide J, Tokunaga T. Rotator cuff tendon-to-bone healing at 12 months after patch grafting of acellular dermal matrix in an animal model. *J Orthop Sci*. 2018;23(2):207-12.

16. Street M, Thambyah A, Dray M, Amirapu S, Tuari D, Callon KE, et al. Augmentation with an ovine forestomach matrix scaffold improves histological outcomes of rotator cuff repair in a rat model. *Journal of Orthopaedic Surgery and Research*. 2015;10.

17. Parisi C, Salvatore L, Veschini L, Serra MP, Hobbs C, Madaghiele M, et al. Biomimetic gradient scaffold of collagen-hydroxyapatite for osteochondral regeneration. *Journal of Tissue Engineering*. 2020;11.

18. Phillips JE, Burns KL, Le Doux JM, Guldberg RE, Garcia AJ. Engineering graded tissue interfaces. *P Natl Acad Sci USA*. 2008;105(34):12170-5.

19. Nukavarapu SP, Dorcenus DL. Osteochondral tissue engineering: Current strategies and challenges. *Biotechnol Adv*. 2013;31(5):706-21.

20. Yang S, Shi X, Li X, Wang J, Wang Y, Luo Y. Oriented collagen fiber membranes formed through counter-rotating extrusion and their application in tendon regeneration. *Biomaterials*. 2019.
21. Choi JS, Kim BS, Kim JY, Kim JD, Choi YC, Yang HJ, et al. Decellularized extracellular matrix derived from human adipose tissue as a potential scaffold for allograft tissue engineering. *J Biomed Mater Res A*. 2011;97a(3):292-9.
22. Kim BS, Choi JS, Kim JD, Yoon HI, Choi YC, Cho YW. Human collagen isolated from adipose tissue. *Biotechnol Prog*. 2012;28(4):973-80.
23. Lipner J, Liu W, Liu Y, Boyle J, Genin GM, Xia Y, et al. The mechanics of PLGA nanofiber scaffolds with biomimetic gradients in mineral for tendon-to-bone repair. *J Mech Behav Biomed*. 2014;40:59-68.
24. Genin GM, Kent A, Birman V, Wopenka B, Pasteris JD, Marquez PJ, et al. Functional grading of mineral and collagen in the attachment of tendon to bone. *Biophys J*. 2009;97(4):976-85.
25. Huang X, Bai S, Lu Q, Liu X, Liu S, Zhu H. Osteoinductive-nanoscaled silk/HA composite scaffolds for bone tissue engineering application. *J Biomed Mater Res B Appl Biomater*. 2015;103(7):1402-14.
26. Cholas R, Padmanabhan SK, Gervaso F, Udayan G, Monaco G, Sannino A, et al. Scaffolds for bone regeneration made of

hydroxyapatite microspheres in a collagen matrix. *Mat Sci Eng C-Mater*. 2016;63:499-505.

27. Gaspar D, Spanoudes K, Holladay C, Pandit A, Zeugolis D. Progress in cell-based therapies for tendon repair. *Adv Drug Deliv Rev*. 2015;84:240-56.

28. Carballo CB, Lebaschi A, Rodeo SA. Cell-based approaches for augmentation of tendon repair. *Tech Shoulder Elb Surg*. 2017;18(3):e6-e14.

29. Mazzocca AD, Chowaniec D, McCarthy MB, Beitzel K, Cote MP, McKinnon W, et al. In vitro changes in human tenocyte cultures obtained from proximal biceps tendon: multiple passages result in changes in routine cell markers. *Knee Surg Sport Tr A*. 2012;20(9):1666-72.

30. Yao L, Bestwick CS, Bestwick LA, Maffulli N, Aspden RM. Phenotypic drift in human tenocyte culture. *Tissue Eng*. 2006;12(7):1843-9.

31. De Miguel MP, Fuentes-Julian S, Blazquez-Martinez A, Pascual CY, Aller MA, Arias J, et al. Immunosuppressive Properties of Mesenchymal Stem Cells: Advances and Applications. *Curr Mol Med*. 2012;12(5):574-91.

32. Sheng HM, Wang Y, Jin YQ, Zhang QY, Zhang Y, Wang L, et al. A critical role of IFN gamma in priming MSC-mediated suppression of T cell proliferation through up-regulation of B7-H1. *Cell*



Res. 2008;18(8):846-57.

33. Omi R, Gingery A, Steinmann SP, Amadio PC, An KN, Zhao C. Rotator cuff repair augmentation in a rat model that combines a multilayer xenograft tendon scaffold with bone marrow stromal cells. *J Shoulder Elbow Surg.* 2016;25(3):469-77.

34. Liu Q, Yu Y, Reisdorf RL, Qi J, Lu C-K, Berglund LJ, et al. Engineered tendon-fibrocartilage-bone composite and bone marrow-derived mesenchymal stem cell sheet augmentation promotes rotator cuff healing in a non-weight-bearing canine model. *Biomaterials.* 2019;192:189-98.

35. Madhurakkat Perikamana SK, Lee J, Ahmad T, Kim EM, Byun H, Lee S, et al. Harnessing biochemical and structural cues for tenogenic differentiation of adipose derived stem cells (ADSCs) and development of an in vitro tissue interface mimicking tendon-bone insertion graft. *Biomaterials.* 2018;165:79-93.

36. Uthoff H, Spenner A, Reckelkamm W, Ahrens B, Wolk G, Hackler R, et al. Critical role of preconceptional immunization for protective and nonpathological specific immunity in murine neonates. *J Immunol.* 2003;171(7):3485-92.

37. Troyer DL, Weiss ML. Concise review: Wharton's jelly-derived cells are a primitive stromal cell population. *Stem Cells.* 2008;26(3):591-9.

38. Hsieh CF, Alberton P, Loffredo-Verde E, Volkmer E,

Pietschmann M, Muller P, et al. Scaffold-free Scleraxis-programmed tendon progenitors aid in significantly enhanced repair of full-size Achilles tendon rupture. *Nanomedicine (Lond)*. 2016;11(9):1153-67.

39. Troyer DL, Weiss ML. Concise review: Wharton's jelly derived cells are a primitive stromal cell population. *Stem Cells*. 2008;26(3):591-9.

40. D'ippolito G, Schiller PC, Ricordi C, Roos BA, Howard GA. Age related osteogenic potential of mesenchymal stromal stem cells from human vertebral bone marrow. *Journal of bone and mineral research*. 1999;14(7):1115-22.

41. Baxter MA, Wynn RF, Jowitt SN, Wraith JE, Fairbairn LJ, Bellantuono I. Study of telomere length reveals rapid aging of human marrow stromal cells following in vitro expansion. *Stem Cells*. 2004;22(5):675-82.

42. Roura S, Farré J, Soler Botija C, Llach A, Hove Madsen L, Cairó JJ, et al. Effect of aging on the pluripotential capacity of human CD105+ mesenchymal stem cells. *European journal of heart failure*. 2006;8(6):555-63.

43. Jo CH, Kim OS, Park EY, Kim BJ, Lee JH, Kang SB, et al. Fetal mesenchymal stem cells derived from human umbilical cord sustain primitive characteristics during extensive expansion. *Cell Tissue Res*. 2008;334(3):423-33.

44. Li M, Luan F, Zhao Y, Hao H, Liu J, Dong L, et al.

Mesenchymal stem cell conditioned medium accelerates wound healing with fewer scars. *International wound journal*. 2017;14(1):64-73.

45. Conconi MT, Burra P, Di Liddo R, Calore C, Turetta M, Bellini S, et al. CD105(+) cells from Wharton's jelly show in vitro and in vivo myogenic differentiative potential. *Int J Mol Med*. 2006;18(6):1089-96.

46. Wu KH, Zhou B, Lu SH, Feng B, Yang SG, Du WT, et al. In vitro and in vivo differentiation of human umbilical cord derived stem cells into endothelial cells. *J Cell Biochem*. 2007;100(3):608-16.

47. Kwon DR, Park GY, Lee SC. Treatment of Full-Thickness Rotator Cuff Tendon Tear Using Umbilical Cord Blood-Derived Mesenchymal Stem Cells and Polydeoxyribonucleotides in a Rabbit Model. *Stem Cells Int*. 2018;2018:7146384.

48. Watkins JP, Auer JA, Gay S, Morgan SJ. Healing of surgically created defects in the equine superficial digital flexor tendon: collagen-type transformation and tissue morphologic reorganization. *Am J Vet Res*. 1985;46(10):2091-6.

49. Ide J, Kikukawa K, Hirose J, Iyama K, Sakamoto H, Mizuta H. The effects of fibroblast growth factor-2 on rotator cuff reconstruction with acellular dermal matrix grafts. *Arthroscopy*. 2009;25(6):608-16.

50. Zhao S, Zhao JW, Dong SK, Huangfu XQ, Bin L, Yang HL,

et al. Biological augmentation of rotator cuff repair using bFGF-loaded electrospun poly(lactide-co-glycolide) fibrous membranes. *Int J Nanomed.* 2014;9:2373-85.

51. Zhao S, Xie XX, Pan GQ, Shen P, Zhao JZ, Cui WG. Healing improvement after rotator cuff repair using gelatin-grafted poly(L-lactide) electrospun fibrous membranes. *J Surg Res.* 2015;193(1):33-42.

52. Benjamin M, Kumai T, Milz S, Boszczyk BM, Boszczyk AA, Ralphs JR. The skeletal attachment of tendons--tendon "entheses". *Comp Biochem Physiol A Mol Integr Physiol.* 2002;133(4):931-45.

53. Galatz LM, Charlton N, Das R, Kim HM, Havlioglu N, Thomopoulos S. Complete removal of load is detrimental to rotator cuff healing. *J Shoulder Elb Surg.* 2009;18(5):669-75.

54. Beck J, Evans D, Tonino PM, Yong S, Callaci JJ. The biomechanical and histologic effects of platelet-rich plasma on rat rotator cuff repairs. *The American journal of sports medicine.* 2012;40(9):2037-44.

55. Kang ES, Ha KY, Kim YH. Fate of transplanted bone marrow derived mesenchymal stem cells following spinal cord injury in rats by transplantation routes. *J Korean Med Sci.* 2012;27(6):586-93.

56. O'Brien FJ, Harley BA, Yannas IV, Gibson LJ. The effect of pore size on cell adhesion in collagen-GAG scaffolds. *Biomaterials.* 2005;26(4):433-41.

57. van Tienen TG, Heijkants RG, Buma P, de Groot JH, Pennings AJ, Veth RP. Tissue ingrowth and degradation of two biodegradable porous polymers with different porosities and pore sizes. *Biomaterials*. 2002;23(8):1731-8.
58. Cao H, Xu SY. EDC/NHS-crosslinked type II collagen-chondroitin sulfate scaffold: characterization and in vitro evaluation. *J Mater Sci Mater Med*. 2008;19(2):567-75.
59. Kim BS, Kim EJ, Choi JS, Jeong JH, Jo CH, Cho YW. Human collagen-based multilayer scaffolds for tendon-to-bone interface tissue engineering. *J Biomed Mater Res A*. 2014;102(11):4044-54.
60. Engler AJ, Sen S, Sweeney HL, Discher DE. Matrix elasticity directs stem cell lineage specification. *Cell*. 2006;126(4):677-89.
61. Tamaddon M, Burrows M, Ferreira SA, Dazzi F, Apperley JF, Bradshaw A, et al. Monomeric, porous type II collagen scaffolds promote chondrogenic differentiation of human bone marrow mesenchymal stem cells in vitro. *Sci Rep-Uk*. 2017;7.
62. Peltz CD, Dourte LM, Kuntz AF, Sarver JJ, Kim SY, Williams GR, et al. The effect of postoperative passive motion on rotator cuff healing in a rat model. *J Bone Joint Surg Am*. 2009;91(10):2421-9.
63. Lipner J, Shen H, Cavinatto L, Liu W, Havlioglu N, Xia Y, et al. In Vivo Evaluation of Adipose-Derived Stromal Cells Delivered with a Nanofiber Scaffold for Tendon-to-Bone Repair. *Tissue Eng Part A*. 2015;21(21-22):2766-74.

64. Chainani A, Little D. Current Status of Tissue-engineered Scaffolds for Rotator Cuff Repair. *Tech Orthop.* 2016;31(2):91-7.
65. Zhang B, Luo Q, Halim A, Ju Y, Morita Y, Song G. Directed Differentiation and Paracrine Mechanisms of Mesenchymal Stem Cells: Potential Implications for Tendon Repair and Regeneration. *Curr Stem Cell Res Ther.* 2017;12(6):447-54.
66. Bianco ST, Moser HL, Galatz LM, Huang AH. Biologics and stem cell-based therapies for rotator cuff repair. *Ann N Y Acad Sci.* 2018;1442(1):35-47.
67. Laranjeira M, Domingues RMA, Costa-Almeida R, Reis RL, Gomes ME. 3D Mimicry of Native-Tissue-Fiber Architecture Guides Tendon-Derived Cells and Adipose Stem Cells into Artificial Tendon Constructs. *Small.* 2017;13(31).
68. Howell K, Chien C, Bell R, Laudier D, Tufa SF, Keene DR, et al. Novel Model of Tendon Regeneration Reveals Distinct Cell Mechanisms Underlying Regenerative and Fibrotic Tendon Healing. *Sci Rep.* 2017;7:45238.
69. Pittenger MF, Mackay AM, Beck SC, Jaiswal RK, Douglas R, Mosca JD, et al. Multilineage potential of adult human mesenchymal stem cells. *Science.* 1999;284(5411):143-7.
70. McGoldrick R, Chattopadhyay A, Crowe C, Chiou G, Hui K, Farnebo S, et al. The Tissue-Engineered Tendon-Bone Interface: In Vitro and In Vivo Synergistic Effects of Adipose-Derived Stem Cells,

Platelet-Rich Plasma, and Extracellular Matrix Hydrogel. *Plast Reconstr Surg*. 2017;140(6):1169-84.

71. Tokunaga T, Karasugi T, Arimura H, Yonemitsu R, Sakamoto H, Ide J, et al. Enhancement of rotator cuff tendon-bone healing with fibroblast growth factor 2 impregnated in gelatin hydrogel sheets in a rabbit model. *J Shoulder Elb Surg*. 2017;26(10):1708-17.

72. Norelli JB, Plaza DP, Stal DN, Varghese AM, Liang H, Grande DA. Tenogenically differentiated adipose-derived stem cells are effective in Achilles tendon repair in vivo. *J Tissue Eng*. 2018;9(1):1-20.

73. Gimbel JA, Van Kleunen JP, Mehta S, Perry SM, Williams GR, Soslowsky LJ. Supraspinatus tendon organizational and mechanical properties in a chronic rotator cuff tear animal model. *J Biomech*. 2004;37(5):739-49.

74. Hernigou P, Flouzat Lachaniette CH, Delambre J, Zilber S, Duffiet P, Chevallier N, et al. Biologic augmentation of rotator cuff repair with mesenchymal stem cells during arthroscopy improves healing and prevents further tears: a case-controlled study. *Int Orthop*. 2014;38(9):1811-8.

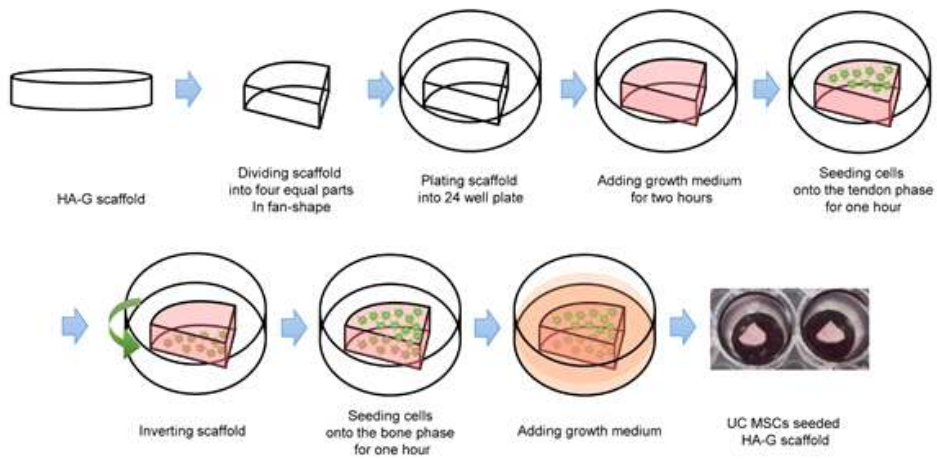
75. Arimura H, Shukunami C, Tokunaga T, Karasugi T, Okamoto N, Taniwaki T, et al. TGF-beta1 Improves Biomechanical Strength by Extracellular Matrix Accumulation Without Increasing the Number of Tenogenic Lineage Cells in a Rat Rotator Cuff Repair Model. *Am J*

Sports Med. 2017;45(10):2394-404.

76. Gao YL, Zhang YQ, Lu YH, Wang Y, Kou XR, Lou Y, et al. TOB1 Deficiency Enhances the Effect of Bone Marrow-Derived Mesenchymal Stem Cells on Tendon-Bone Healing in a Rat Rotator Cuff Repair Model. *Cell Physiol Biochem*. 2016;38(1):319-29.

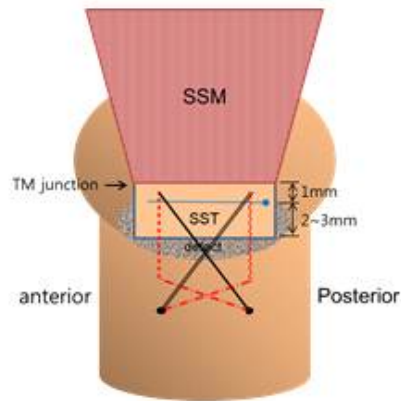
77. Tokunaga T, Shukunami C, Okamoto N, Taniwaki T, Oka K, Sakamoto H, et al. FGF-2 Stimulates the Growth of Tenogenic Progenitor Cells to Facilitate the Generation of Tenomodulin-Positive Tenocytes in a Rat Rotator Cuff Healing Model. *Am J Sport Med*. 2015;43(10):2411-22.



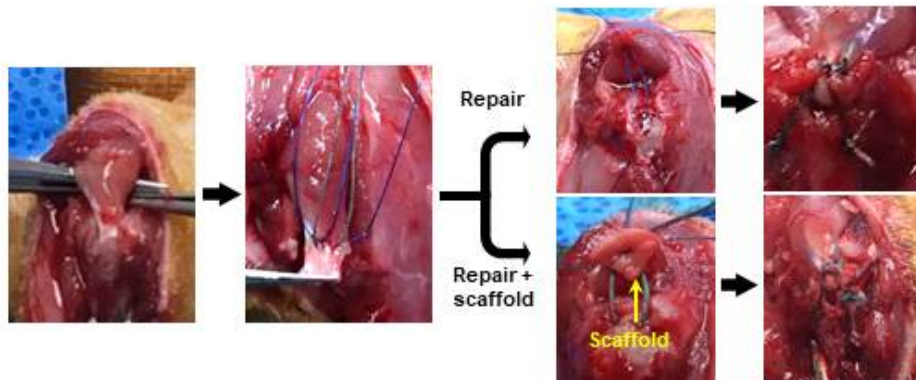


**Figure 1** Procedure of UC MSCs seeding to the HA-G scaffold. Abbreviations: HA-G, hydroxyapatite gradient. UC MSCs, umbilical cord derived mesenchymal stem cells.

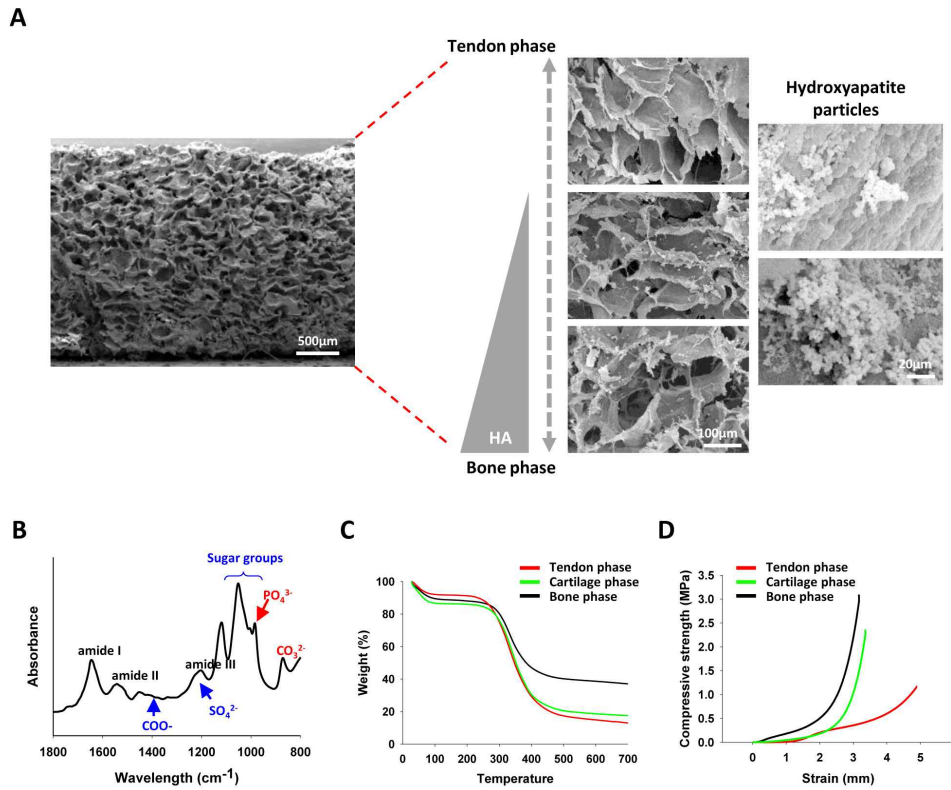
**A**



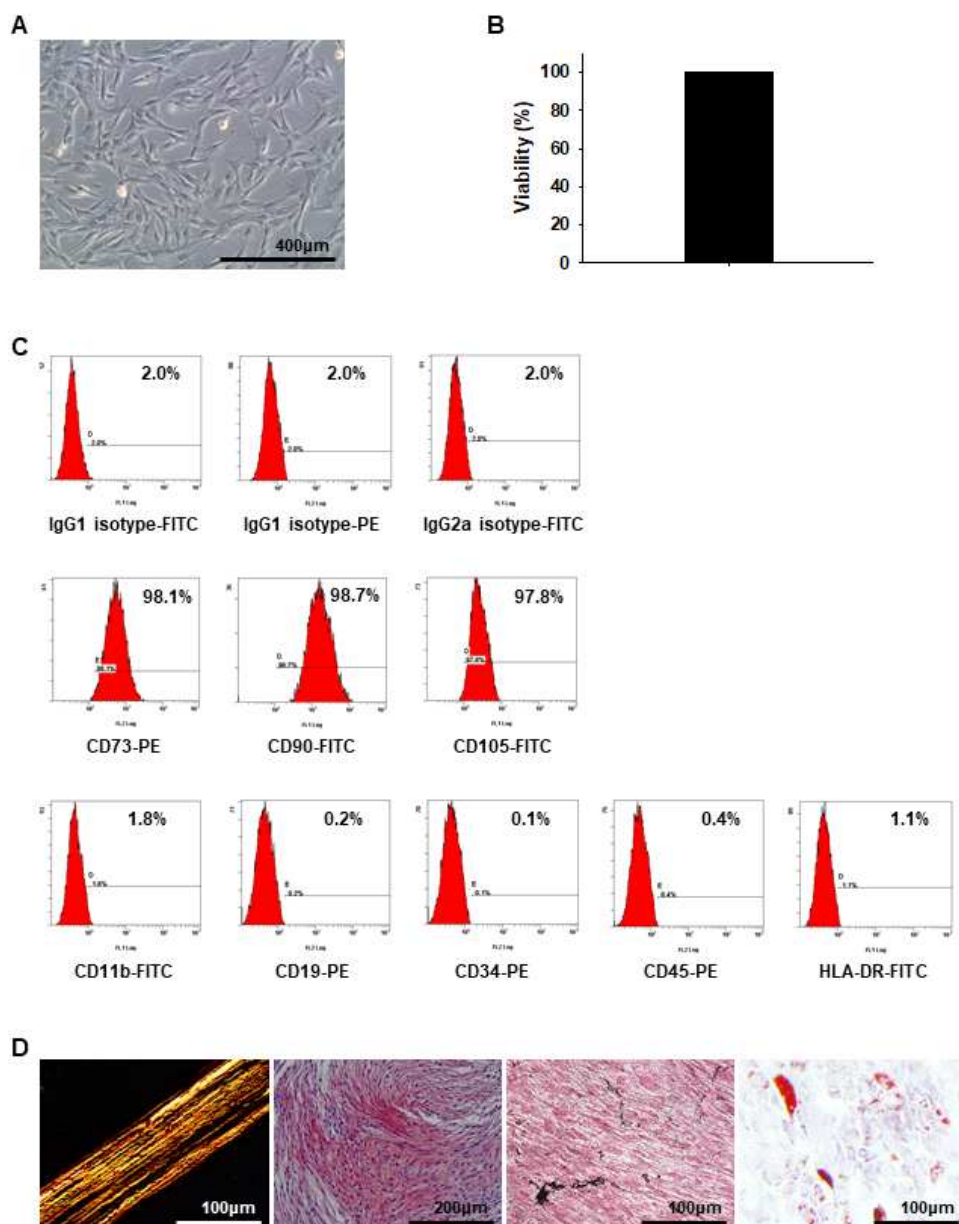
**B**



**Figure 2** Surgical procedure of rotator cuff tendon repair. (A) Schematic image of repair surgery. (B) Surgical procedure of rotator cuff tendon repair and implantation of scaffold with repair. Abbreviations: SSM, supraspinatus muscle. SST, supraspinatus tendon. TM, tendon muscular.

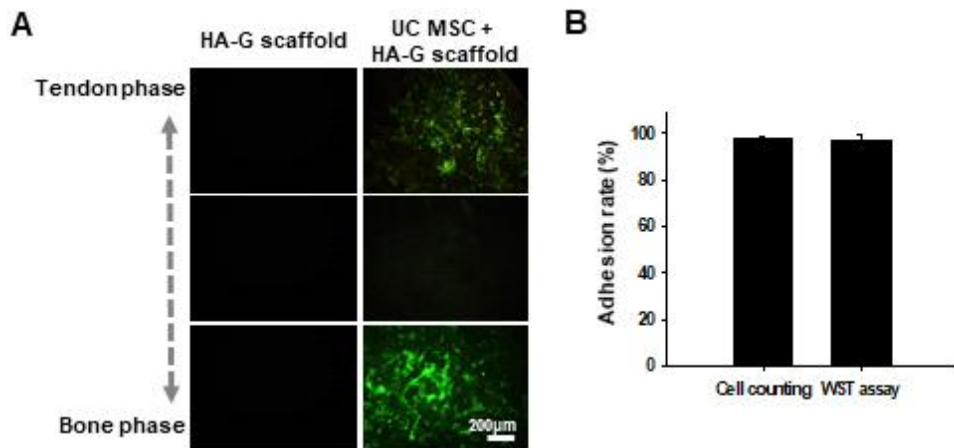


**Figure 3** Characterization of the HA-G scaffold. (A) SEM image of the scaffold with HA particles gradient concentrations. (B) Absorption bands of the scaffold by FTIR spectrophotometry. (C) Weight loss of the three parts in the HA-G scaffold measured by TGA. (D) Compressive strength of the three parts in the HA-G scaffold. Abbreviations: HA, hydroxyapatite. HA-G, hydroxyapatite gradient. SEM, scanning electron microscopy. FTIR, Fourier-transform infrared. TGA, thermogravimetric analysis.

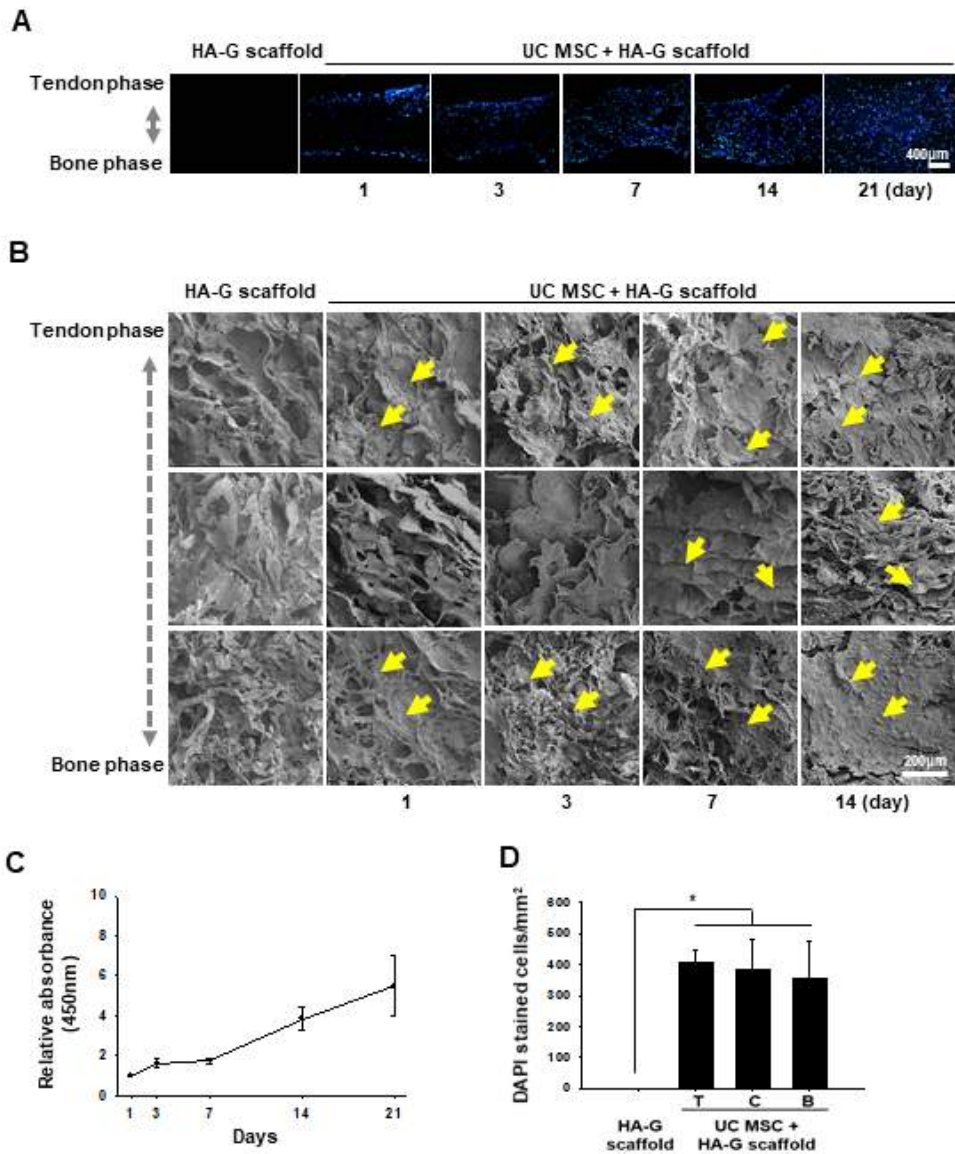


**Figure 4** Characterization of UC MSCs at passage 10. (A) Morphology of Cells. (B) Viability of cells. (C) Flow-cytometric results of cells: isotype controls were IgG1 isotype-FITC, IgG1 isotype-PE and IgG2a isotype-FITC, positive markers were CD73-PE, CD90-FITC and CD105-FITC, and negative

markers were CD11b-FITC, CD19-PE, CD34-PE, CD45-PE and HLA-DR-FITC. (D) Tenogenic, chondrogenic, osteogenic and adipogenic differentiation of UC MSCs by stainings with PSR, Saf-O, Von Kossa and Oil Red O. Abbreviations: UC MSCs, umbilical cord derived mesenchymal stem cells; PSR, picrosirius red, Saf-O, safranin-O/fast green.



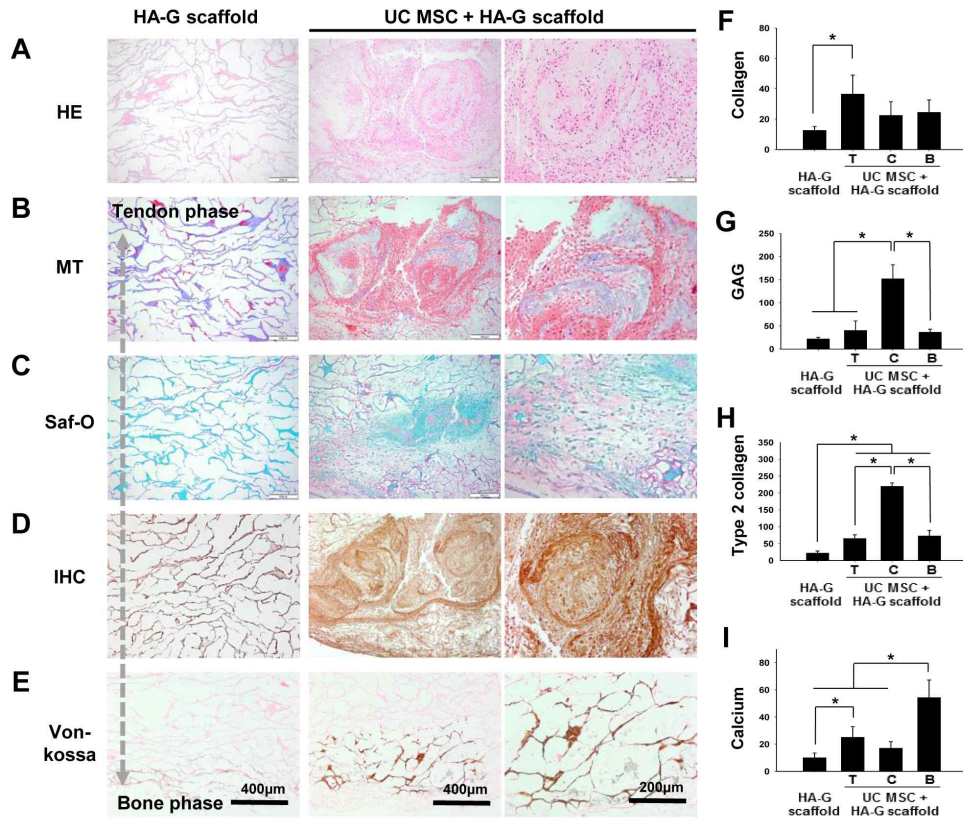
**Figure 5** Adhesion of UC MSCs to the HA-G scaffold. (A) Calcein-AM staining of the HA-G scaffold and UC MSC + HA-G scaffold for cell adhesion to the scaffold at 24 hours. (B) Adhesion rate by counting cell numbers and by the WST assay at 24 hours. Abbreviations: HA-G, hydroxyapatite gradient. UC MSCs, umbilical cord derived mesenchymal stem cells.



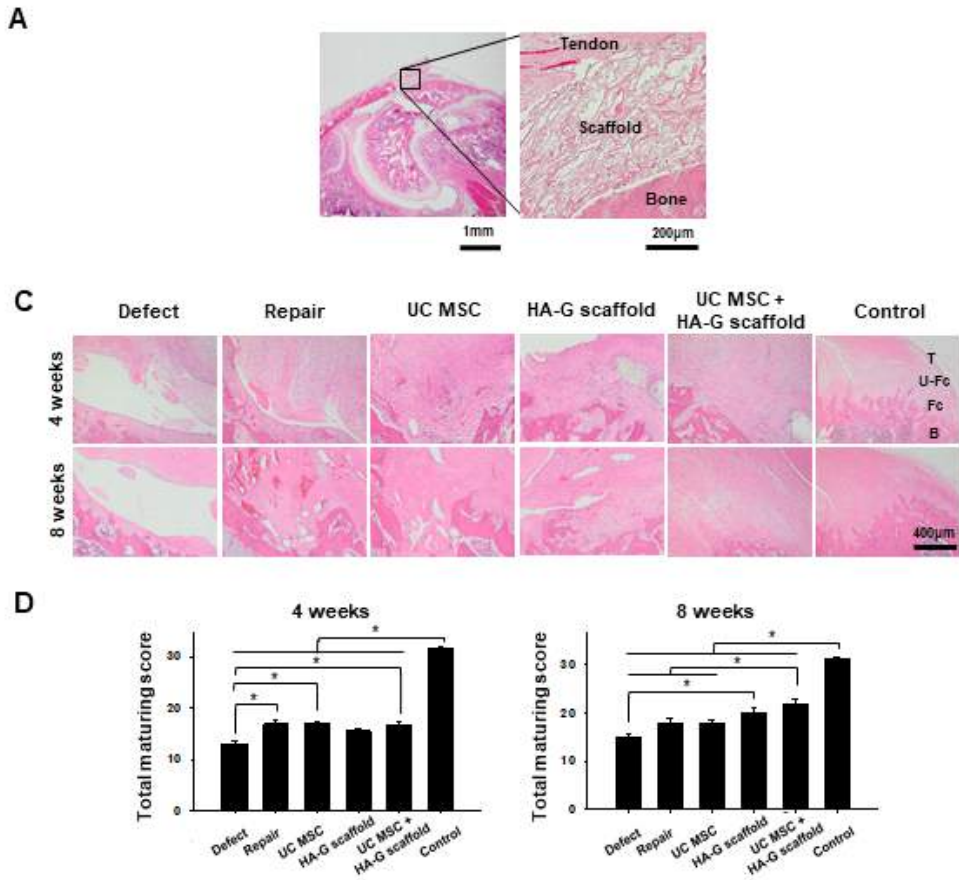
**Figure 6** Infiltration, and proliferation of UC MSCs in the HA-G scaffold. (A) DAPI staining of the HA-G scaffold and UC MSC + HA-G scaffold for cell infiltration from the surface to the center of the scaffold at 1, 3, 7 and 14 days. (B) SEM image of the HA-G scaffold and UC MSC + HA-G scaffold at days 1, 3, 7, and 14 days (yellow arrows indicate UC MSCs). (C)

Proliferation kinetics of UC MSCs cultured in the HA-G scaffold at 1, 3, 7, 14 and 21 days using WST assay. (D) DAPI stained cells/mm<sup>2</sup> in HA-G scaffold and UC MSC + HA-G scaffold at tendon, cartilage and bone phase respectively at 21days. The bar charts represent the mean  $\pm$  standard deviation. Abbreviations: HA-G, hydroxyapatite gradient. UC MSC, umbilical cord-derived mesenchymal stem cell. WST, water-soluble tetrazolium salt. SEM, scanning electron microscopy.

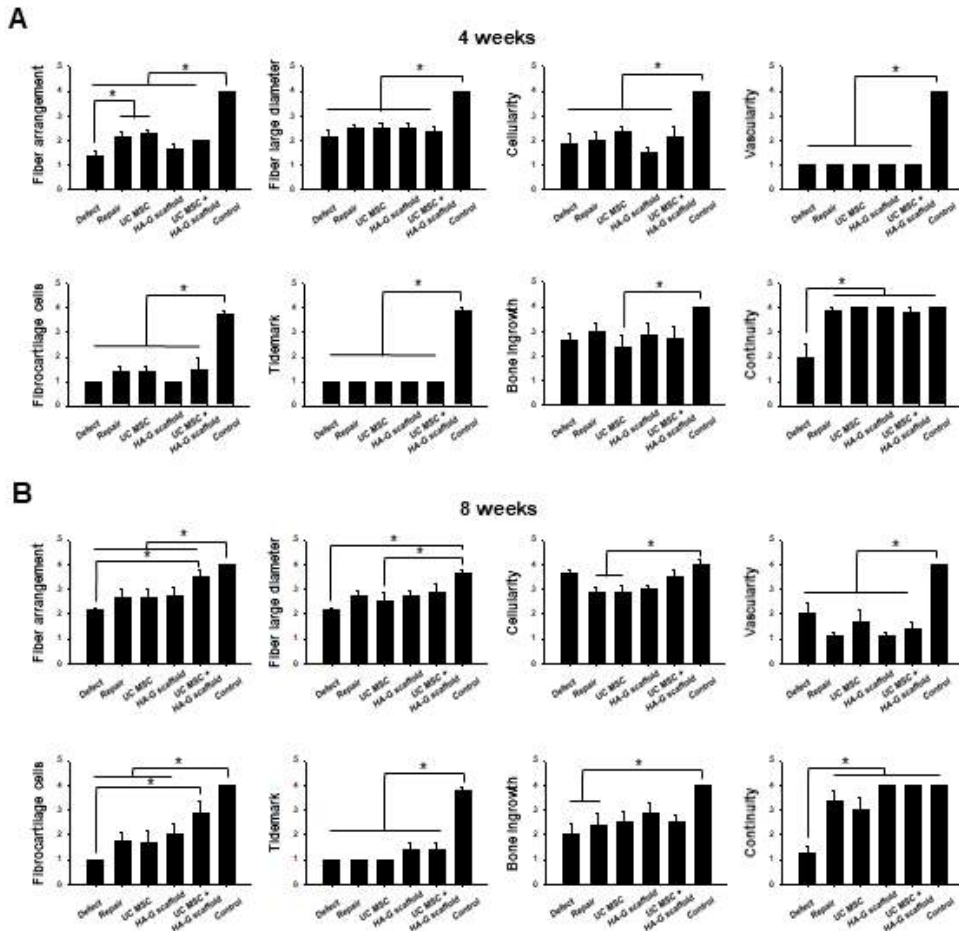




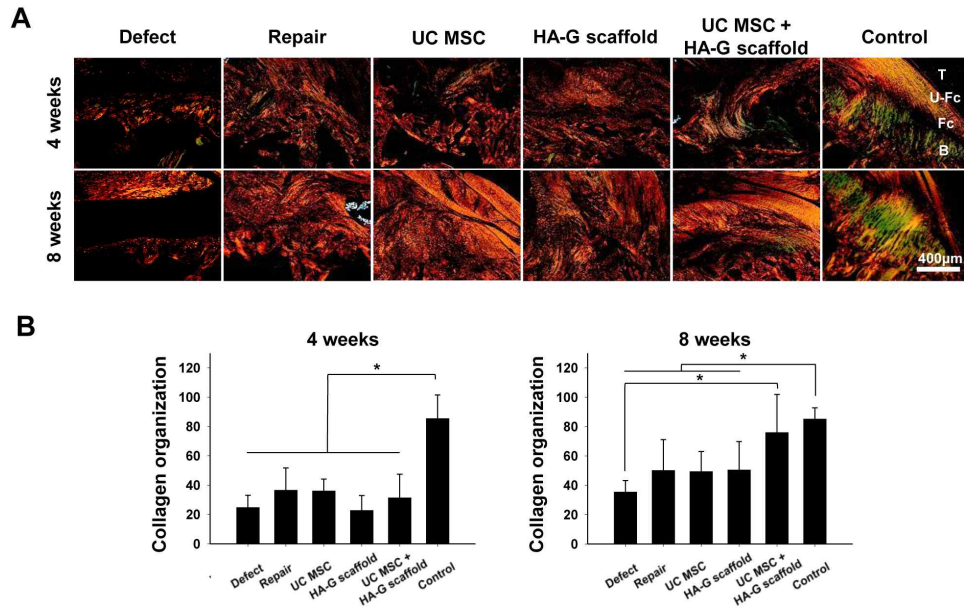
**Figure 7** Differentiation of UC MSCs in the HA-G scaffold at tendon, cartilage and bone phase at 28 days. (A) HE staining, (B) MT staining, (C) Saf-O staining, (D) IHC staining of type 2 collagen, and (E) Von-kossa staining in the HA-G scaffold and the UC MSC + HA-G scaffold. (F) Area of collagen. (G) Area of GAG. (H) Area of type 2 collagen. (I) Area of calcium. The bar charts represent the mean  $\pm$  standard deviation; statistically significant at  $p < 0.05$ . Abbreviations: HA-G, hydroxyapatite gradient. UC MSC, umbilical cord-derived mesenchymal stem cell. HE, hematoxylin and eosin. MT, Masson's trichrome. Saf-O, safranin-O/fast green. GAG, glycosaminoglycan. IHC, immunohistochemistry. T, tendon phase. C, cartilage phase. B, bone phase.



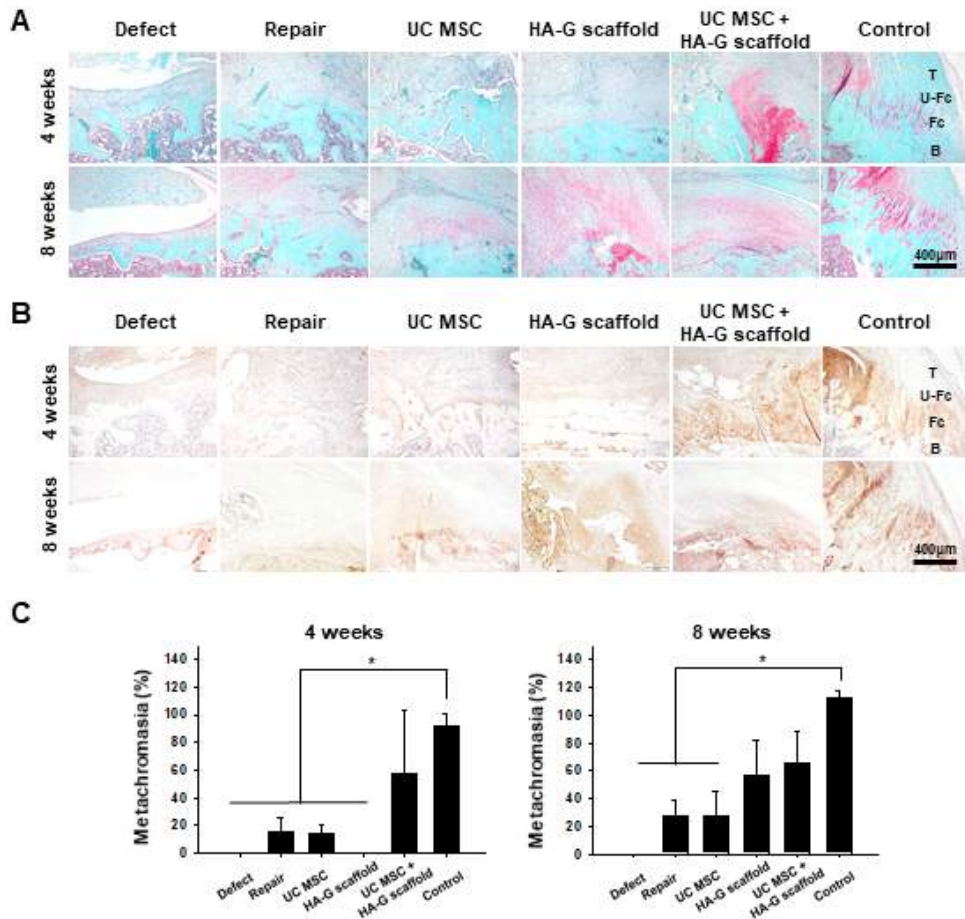
**Figure 8** Histologic image of the general structure, and quantification of the changes in the TBI at 4 and 8 weeks. (A) The inserted scaffold settled into the right place between the SST and the bone. (B) HE staining of TBI at 4 and 8 weeks. (C) Total regeneration score at 4 and 8 weeks. The bar charts represent the mean  $\pm$  standard deviation: statistically significant at  $p < 0.05$ . Abbreviations: UC MSC, umbilical cord-derived mesenchymal stem cell. HA-G, hydroxyapatite gradient. T, tendon. U-Fc, uncalcified fibrocartilage. Fc, calcified fibrocartilage. B, bone. SST, supraspinatus tendon. HE, hematoxylin and eosin.



**Figure 9** Detail parameters of total regeneration score of TBI. (A) Detailed parameters at 4 weeks. (B) Detailed parameters at 8 weeks. The bar charts represent the mean  $\pm$  standard deviation; statistically significant at  $p < 0.05$ . Abbreviations: UC MSC, umbilical cord-derived mesenchymal stem cell. HA-G, hydroxyapatite gradient. TBI, tendon-to-bone interface.

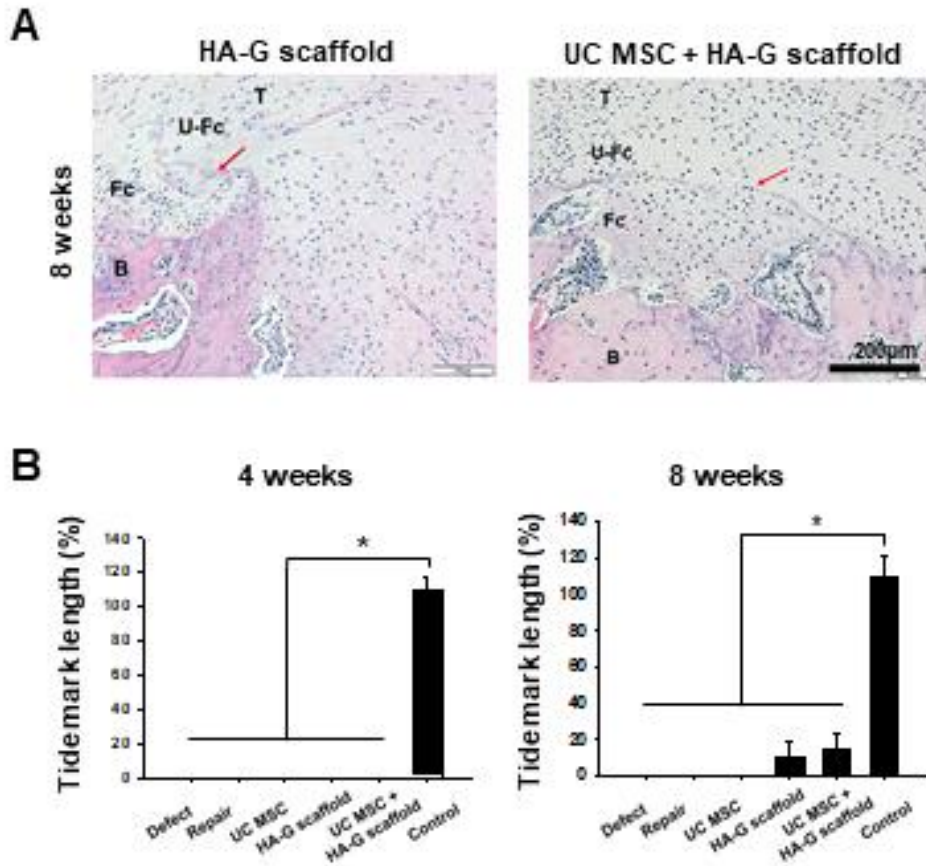


**Figure 10** Representative histologic images of the collagen matrix and quantification of the changes in the TBI at 4 and 8 weeks. (A) PSR staining of TBI at 4 and 8 weeks. (B) Collagen organization in all groups at 4 weeks and 8 weeks. The bar charts represent the mean  $\pm$  standard deviation; statistically significant at  $p < 0.05$ . Abbreviations: UC MSC, umbilical cord-derived mesenchymal stem cell. HA-G, hydroxyapatite gradient. T, tendon. U-Fc, uncalcified fibrocartilage. Fc, calcified fibrocartilage. B, bone. TBI, tendon-to-bone interface. PSR, picrosirius red.

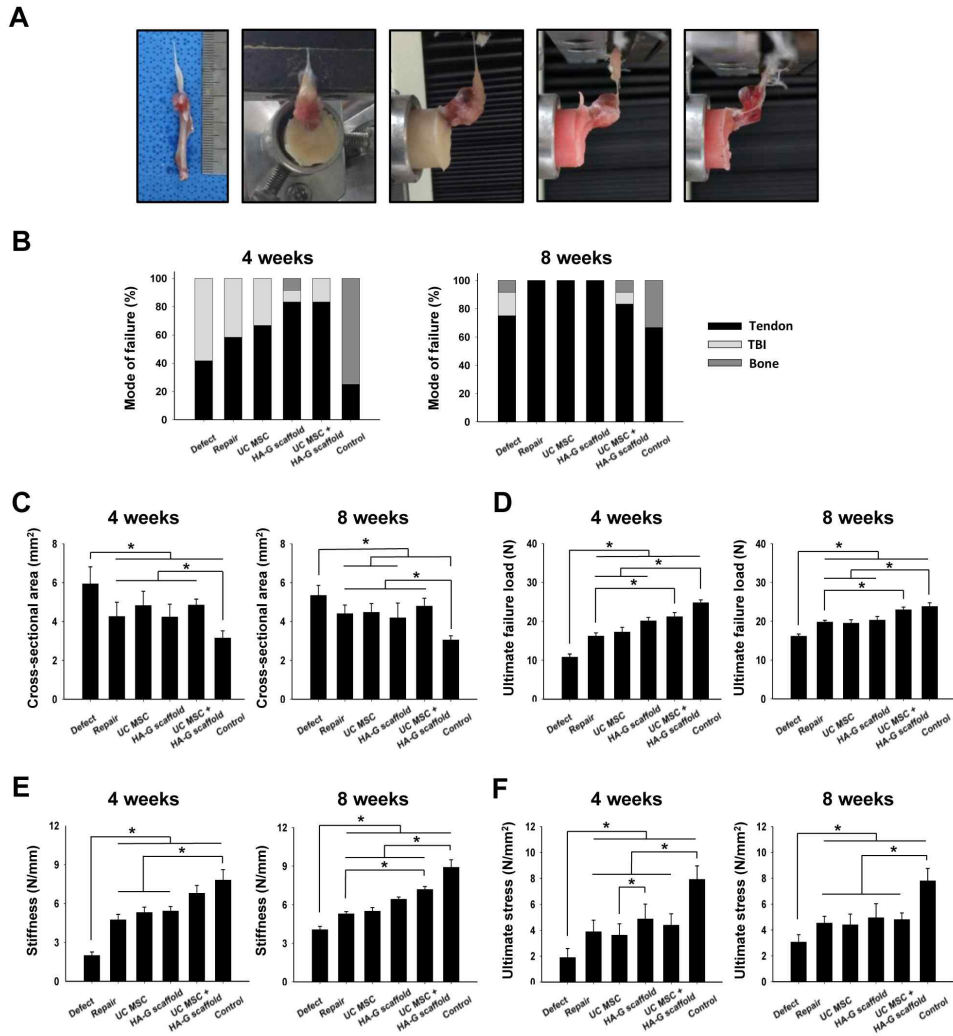


**Figure 11** Representative histologic images of cartilage and quantification of the changes in TBI at 4 and 8 weeks. (A) Saf-O staining of TBI in all groups at 4 and 8 weeks. (B) IHC staining of type II collagen of TBI in all groups at 4 and 8 weeks. (C) The relative area of metachromasia at 4 and 8 weeks. The bar charts represent the mean  $\pm$  standard deviation; statistically significant at  $p < 0.05$ . Abbreviations: UC MSC, umbilical cord-derived mesenchymal stem cell. HA-G, hydroxyapatite gradient. T, tendon. U-Fc, uncalcified fibrocartilage. Fc, calcified fibrocartilage. B, bone. Saf-O, safranin-O/fast green. TBI, tendon-to-bone interface. GAG, glycosaminoglycan.





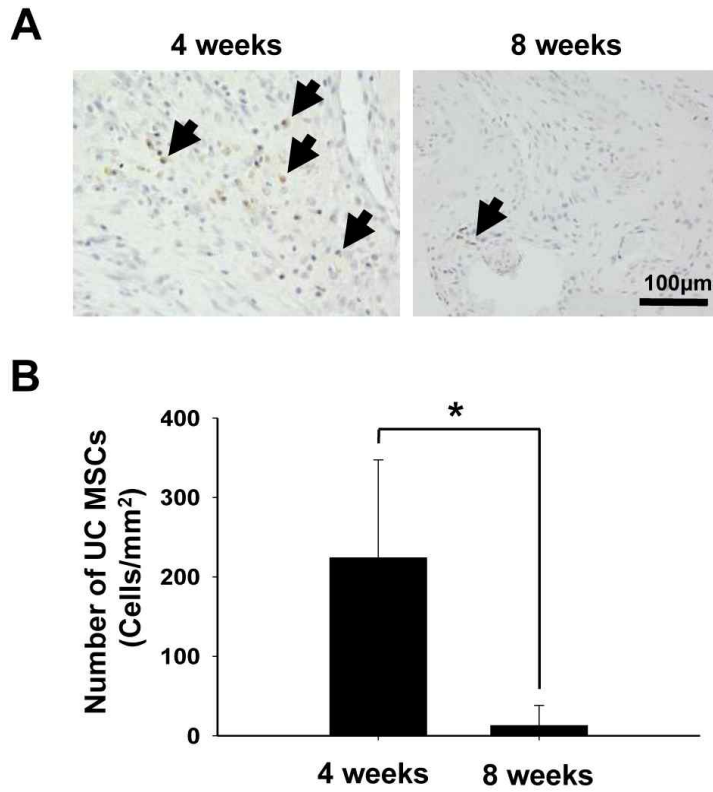
**Figure 12** Representative histologic images of tidemark and quantification of the changes in TBI at 4 and 8 weeks. (A) The tidemark between calcified fibrocartilage and uncalcified fibrocartilage in the HA-G scaffold and the UC MSC + HA-G scaffold groups at 8 weeks. (B) The relative tidemark length in all groups at 4 and 8 weeks. Abbreviations: UC MSC, umbilical cord-derived mesenchymal stem cell. HA-G, hydroxyapatite gradient. T, tendon. U-Fc, uncalcified fibrocartilage. Fc, calcified fibrocartilage. B, bone. TBI, tendon-to-bone interface.



**Figure 13** Biomechanical test procedure and quantification of biomechanical properties of TBI at 4 and 8 weeks. (A) Biomechanical testing procedure and failure cases: an extracted specimen, specimen fixation to the material testing system before tensile loading, a case of failure of the tendon, a case of failure of the TBI, a case of failure of the bone. (B) Incidence of failure for tendons, TBI and bone, respectively, at 4 weeks (left) and 8 weeks (right). (C) Cross-sectional area, (D) ultimate failure load, (E) stiffness, and

(F) ultimate stress for all groups at 4 and 8 weeks. The bar charts represent the mean  $\pm$  standard deviation; statistically significant at  $P < 0.05$ . Abbreviations: UC MSC, umbilical cord-derived mesenchymal stem cell. HA-G, hydroxyapatite gradient. TBI, tendon-to-bone interface.





**Figure 14** Representative trafficking image of the human UC MSCs implanted within the TBI and quantification of the cells at 4 and 8 weeks. (A) IHC staining with human mitochondrial antibody in the TBI at 4 and 8 weeks (black arrows indicate DAB-stained UC MSCs). (B) Number of UC MSCs per area in the TBI. The bar charts represent the mean  $\pm$  standard deviation; statistically significant at  $p < 0.05$ . Abbreviations: UC MSC, umbilical cord-derived mesenchymal stem cell. IHC, immunohistochemistry. TBI, tendon-to-bone interface.

## 요약(국문초록)

# 제대유래 중간엽 줄기세포를 적용한 수산화인회석 농도 경사 세포외기질 스캐폴드의 회전근개 건-골 접합부 재생 효과

예지혜

서울대학교 대학원

의학과 중재의학 전공

회전근개 건-골 접합부의 농도 경사 구조 재생은 회전근개 치료의 궁극적인 목표이다. 본 연구에서는 건-골 접합부의 구조를 재연한 수산화인회석 농도 경사 세포외기질 (HA-G) 스캐폴드에 제대유래 중간엽 줄기세포를 적용하여 건-골 접합부의 조직 재생을 분석함으로써 그 유효성을 규명하고자 한다.

본 연구에서는 인간 지방조직의 세포외기질을 분리하여 세포외기질 스캐폴드를 제작하고 그 위를 연골의 구성 성분인 콘드로이틴황아염으로 코팅했다. 그 후, 디핑 방법을 통하여 수산화인회석을 농도 경사지게 형성함으로써 건-골 접합부 유사구조로 HA-G 스캐폴드를 제작했다. 제작된 스캐폴드는 높은 구조적 상호연결성을 보였으며, 공극크기는 100~150  $\mu\text{m}$  이고 공극률은 91%이었다. 이 스캐폴드는 건쪽에 비해 연골과 골쪽에서 수산화인회석의 비율이 각 1.4배와 2.9배 높았으며, 기계

적 강도 또한 각 1.5배와 2.3배 높았다.

HA-G 스캐폴드의 양쪽 표면에 제대유래 중간엽 줄기세포를 적용하여 세포 부착을 확인한 결과 24시간 후 건쪽과 골쪽의 표면에 세포 부착률은 98%이었다. 부착 후 7일에는 스캐폴드의 내부까지 세포가 이동했으며, 14일에는 건, 연골 그리고 골 측면에 세포가 고르게 분포했다. 증식률은 1일에 비해 7일에 1.8배, 21일에는 6배에 달했다.

제대유래 중간엽 줄기세포 부착 4주 후, 건 그리고 연골, 골 부분으로 나눠 조직학적 분석을 진행한 결과, HA-G 스캐폴드군에 비하여 줄기세포를 적용한 HA-G 스캐폴드군에서 콜라겐 침착이 건 측면에 2.9배, 글리코사미노글리칸 침착이 연골 측면에 6.3배 그리고 칼슘 침착이 골 측면에서 5.4배 각각 유의하게 증가했다 ( $p < 0.001$ ).

제대유래 중간엽 줄기세포를 적용한 HA-G 스캐폴드를 회전근개 파열 복원 모델에 적용한 결과, 단순 복원 그룹(대조군)에 비하여 조직의 성숙 점수가 중간엽 줄기세포를 적용한 HA-G 스캐폴드 군(실험군)에서 8주에 1.2배 유의하게 향상되었다 ( $p = 0.021$ ). 또한 콜라겐 형성이 8주에 1.6배 그리고 연골 형성이 4주에 3.8배 향상되었다. 특히 연골 성숙 단계에서만 확인할 수 있는 tidemark가 대조군에서 발견되지 않은 반면에 실험군에서 8주에 14% 재생되었다.

건의 기능적 회복 평가로 생역학 실험을 진행한 결과, 궁극적 파열 부하 값이 단순 복원 그룹에 비하여 실험군에서 4주에 1.3배 유의하게 증가했으며, 8주에는 1.2배 유의하게 증가했다 (각  $p = 0.004$ ,  $p = 0.049$ ). 강직 값 또한 8주에 1.7배 유의하게 증가했으며 ( $p = 0.001$ ), 이 결과 값들은 정상 건 그룹과도 유의한 차이가 없었다.

결론적으로 본 연구는 수산화인회석 농도 경사가 형성된 스캐폴드에 중간엽 줄기세포를 적용하여 건, 연골 및 골 기질이 순차적으로 형성된 것

을 확인하였고, 이러한 중간엽 줄기세포를 적용한 HA-G 스캐폴드는 랫트 회전근개 복원술 모델의 건-골 접합부 재생을 조직학적 및 생역학적 측면에서 유도함을 증명하였다. 본 연구의 결과는 향후 회전근개 질환의 근본적인 치료 방법에 중요한 근거로 사용될 수 있을 것이라 기대된다.<sup>1)</sup>

.....

**주요어 :** 어깨 통증, 회전근개, 건-골 접합부, 제대, 중간엽 줄기세포, 농도 경사 스캐폴드, 지방조직

**학번 :** 2017-32957

---

1) 본 내용은 아래의 논문으로 게재됨.

Yea J-H et al., Regeneration of the Rotator Cuff Tendon-to-Bone Interface using Umbilical Cord-Derived Mesenchymal Stem Cells and Gradient Extracellular Matrix Scaffolds from Adipose Tissue in a Rat Model. Acta Biomaterialia. 2020;114:104-116